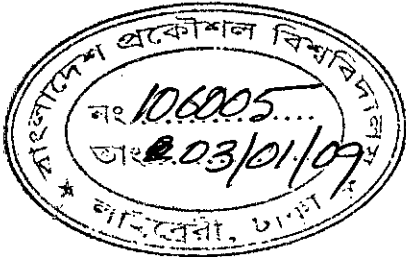


# PERFORMANCE ANALYSIS OF A FREE-SPACE OPTICAL COMMUNICATION SYSTEM THROUGH ATMOSPHERIC TURBULENCE CHANNELS

by

Md. Nazmul Alam



Under the supervision of  
Professor Satya Prasad Majumder

A thesis submitted in partial fulfillment of the requirement for the degree of

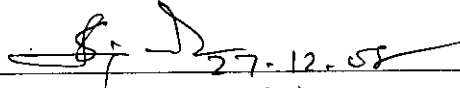
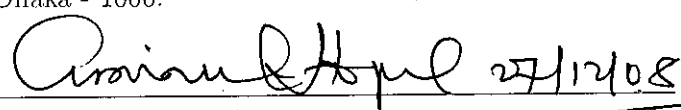
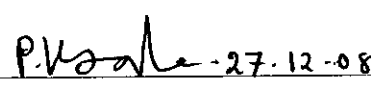
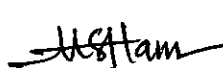
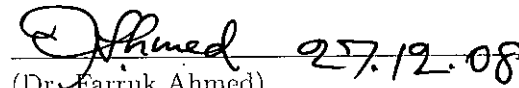
MASTER OF SCIENCE  
IN  
ELECTRICAL AND ELECTRONIC ENGINEERING



DEPARTMENT OF ELECTRICAL AND ELECTRONIC ENGINEERING  
BANGLADESH UNIVERSITY OF ENGINEERING AND TECHNOLOGY  
December 2008

The thesis entitled "Performance Analysis of a Free-space Optical Communication System Through Atmospheric Turbulance Channels" submitted by Md. Nazmul Alam Roll No.: 100606219P, Session: October, 2006 has been accepted as satisfactory in partial fulfillment of the requirements for the degree of Master of Science in Electrical and Electronic Engineering on December 27, 2008.

BOARD OF EXAMINERS

1.  27.12.08  
Chairman  
(Dr. Satya Prasad Majumder)  
*Professor*  
Department of Electrical and Electronic Engineering  
Bangladesh University of Engineering and Technology  
Dhaka - 1000.
2.  27/12/08  
Member  
(Ex-officio)  
(Dr. Aminul Hoque)  
*Professor and Head*  
Department of Electrical and Electronic Engineering  
Bangladesh University of Engineering and Technology  
Dhaka - 1000.
3.  27.12.08  
Member  
(Dr. Pran Kanai Saha )  
*Professor*  
Department of Electrical and Electronic Engineering  
Bangladesh University of Engineering and Technology  
Dhaka - 1000.
4.   
Member  
(Dr. Shah Alam)  
*Associate Professor*  
Department of Electrical and Electronic Engineering  
Bangladesh University of Engineering and Technology  
Dhaka - 1000.
5.  27.12.08  
Member  
(External)  
(Dr. Farruk Ahmed)  
*Professor*  
Department of CSE, North South University  
(Ex Professor, Dept. of Applied Physics & Electronics  
University of Dhaka)

# Declaration

It is hereby declared that this thesis or any part of it has not been submitted elsewhere for the award of any degree or diploma.

Signature of the candidate

*Nazmul Alam*

---

(Md. Nazmul Alam)

# Dedication

*To my beloved parents.*

# Acknowledgements

I would like to commence this thesis by expressing my gratitude towards Almighty *Allah, Who* blessed me with *His* endless mercy, *Filled* me with diligence and perseverance. It is a great pleasure to express indebtedness gratitude and profound respect to my supervisor Prof. Satya Prasad Majumder for his consistent guidance, relentless encouragement, helpful suggestions, constructive criticism and endless patience throughout the progress of this research. The successful completion of this thesis would not have been possible without persistent motivation and continuous guidance of my honorable supervisor.

The author is also grateful to Dr. Aminul Hoque, Professor and Head, Department of Electrical and Electronic Engineering, Bangladesh University of Engineering and Technology (BUET), Dhaka, for providing valuable suggestions on writing a satisfactory thesis.

I also express my profound indebtedness to Prof.M. Rezwan Khan, Vice Chancellor of UIU for his encouragement and research facilities.

Special thanks to my friend Md. Itrat Bin Shams, Lecturer, Department of EEE, BUET for his continuous support.

And last but not the least, I would be eternally grateful to my parents and brothers because of their incessant passion, encouragement and support. I humbly dedicate this thesis to them.

# Contents

Approval	i
Declarartion	ii
Acknowledgements	iv
Contents	iv
List of Abbreviations	viii
List of Figures	ix
List of Tables	xii
<b>1 Introduction</b>	<b>2</b>
1.1 General Perspective	2
1.2 Brief History of Optical Wireless Communication	3
1.3 Objective of The Thesis	4
1.4 Organization of This Thesis	4
<b>2 Basic Knowledge of Optical Wireless Communication Systems</b>	<b>6</b>
2.1 Introduction	6
2.2 Importance of Free-Space Optical Communication in Communica- tion System	6
2.3 Brief Description of Major Components of a Optical Wireless Link	8
2.3.1 Optical Sources	8
2.3.2 Optical Detectors	9
2.4 Channel Topologies	10
2.4.1 Point-to-point Links	10

2.4.2	Diffuse Links	12
2.4.3	Quasi-Diffuse Links	13
2.4.4	Comparison of Different Technologies	14
2.5	Eye and Skin Safety	15
<b>3</b>	<b>Distribution Models for Turbulence-Induced Intensity Fading</b>	<b>18</b>
3.1	Log-normal pdf	18
3.1.1	Marginal Distribution of Fading	18
3.1.2	Joint Spatial and Temporal Distributions of Fading	20
3.2	Gamma-gamma Distribution	21
3.3	Comparison	22
<b>4</b>	<b>Performance Analysis</b>	<b>26</b>
4.1	Introduction	26
4.2	Block Diagram of the Free-space Optical Communication System	26
4.3	Performance Analysis for OOK for Log-normal Turbulence Condition	27
4.3.1	System Model for OOK	27
4.3.2	Performance Analysis for Log-normal Turbulence Channel	28
4.3.3	Performance Analysis for Log-normal Turbulence Channel in Spatial Diversity Reception	29
4.4	Free Space Optical Communications Systems Employing Subcarrier PSK	31
4.4.1	Free Space Optical Communications Systems Employing Subcarrier PSK Through Turbulent Atmospheric Channel for Log-normal PDF Channel	31
4.4.2	Free Space Optical Communications Systems Employing Subcarrier PSK Through Turbulent Atmospheric Channel for Gamma-Gamma PDF Channel	33
4.5	ML Detection of Q-Ary PPM in Turbulence Channels	33
4.5.1	QPPM Modulation	33
4.5.2	Optical Detection in QPPM	35
4.6	Performance Analysis for Log-normal Turbulence Channel	38
4.7	Performance Analysis and Numerical Results for Gamma-Gamma Turbulence Channel	40

<b>5</b>	<b>Result and Discussion</b>	<b>42</b>
5.1	Introduction	42
5.2	Performance analysis for OOK	43
5.2.1	Performance Analysis for OOK in Log-normal Turbulence Condition for Single Receiver	43
5.2.2	Performance Analysis for OOK in Log-normal Turbulence Condition for Dual Receiver	48
5.3	Free Space Optical Communications Systems Employing Subcar- rier PSK	50
5.3.1	Free Space Optical Communications Systems Employing Subcarrier PSK Through Turbulent Atmospheric Channel for Log-normal channel	50
5.3.2	Free Space Optical Communications Systems Employing Subcarrier PSK Through Turbulent Atmospheric Channel for Gamma-Gamma Channel	55
5.4	Performance Analysis for Q-ary PPM	57
5.4.1	Numerical Result and Discussion for Log-normal Channel	57
5.4.2	Numerical Result and Discussion for Gamma-gamma Channel	59
<b>6</b>	<b>Conclusion</b>	<b>61</b>
6.1	Summary	61
6.2	Scope of Future Research Work	62



# List of Abbreviations

<b>SNR</b>	Signal to noise ratio
<b>SI</b>	Scintillation index
<b>FSO</b>	Free-space optical
<b>BER</b>	Bit error rate
<b>SEP</b>	Symbol error probability
<b>BPSK</b>	Binary phase shift keying
<b>QPSK</b>	Quadrature Phase shift keying
<b>MIMO</b>	Multiple-input multiple-output
<b>PPM</b>	Pulse position modulation
<b>FOV</b>	Field of View
<b>IEC</b>	International Electrotechnical Commission
<b>ANSI</b>	American National Standards Institute
<b>AEL</b>	Allowable Exposure Limit
<b>OOK</b>	On Off Keying

# List of Figures

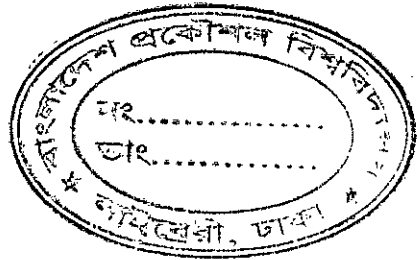
Fig. 2.1 Block diagram of optical intensity, direct detection communication channel.	8
Fig. 2.2 Block diagram of point to point optical link	11
Fig. 2.3 A diffuse optical wireless communication system	13
Fig. 2.4 A quasi-diffuse optical wireless communication system	14
Fig. 3.1 Standard deviation of the log-amplitude fluctuation versus propagation distance for a plane wave.	23
Fig. 3.2 Log-normal and Rayleigh pdfs	23
Fig. 3.3 Distribution of intensity fluctuations for several values of the turbulence strength	24
Fig. 3.4 Distribution of intensity fluctuations for several values of the SI	24
Fig. 3.5 Distribution of intensity fluctuations for different models	25
Fig. 4.1 Block Diagram of an Optical Communication System Through Atmospheric Turbulence Channel	27
Fig. 4.2 Dual branch reception on atmospheric turbulence channels with correlated turbulence-induced fading equal-gain combining with threshold detection	30
Fig. 4.3 Block diagram Q-ary PPM MIMO system	33
Fig. 5.1 Threshold versus normalized received signal amplitude for different values of the log-amplitude standard deviation for $N/2=.01$ .	43
Fig. 5.2 Likelihood ratio versus normalized received signal amplitude for different values of the log-amplitude standard deviation for $N/2=.005$ .	43
Fig. 5.3 Normalized threshold versus log-amplitude standard deviation for different values of the noise covariance.	44

Fig. 5.4 BER vs average signal to noise ratio (SNR) for different $\sigma_x$	45
Fig. 5.5 BER vs average signal to noise ratio (SNR) for different S.I.	45
Fig. 5.6 Minimum SNR required for maintaining BER of $10^{-6}$	46
Fig. 5.7 BER vs $I_0$ for different $\sigma_x$ where $N/2=0.001$	46
Fig. 5.8 BER vs $I_0$ for different $\sigma_x$ where $N/2=0.01$	47
Fig. 5.9 Bit error rate of dual branch receiver versus signal-to-noise ratio using EGC receiver for different value of $p_d$ for $\sigma_x=0.25$	48
Fig. 5.10 Bit error rate of dual branch receiver versus signal-to-noise ratio using EGC receiver for different value of $p_d$ for $\sigma_x=0.1$ .	48
Fig. 5.11 BER performance of optical communication systems employing subcarrier BPSK for different $\sigma_x$ for log-normal turbulence channel	50
Fig. 5.12 BER performance of optical communication systems employing subcarrier BPSK for different S.I. for log-normal turbulence channel	51
Fig. 5.13 Minimum SNR required for maintaining BER of $10^{-6}$ BPSK modulation scheme for log-normal turbulence channel	51
Fig. 5.14 Comparison of BER performance of subcarrier BPSK and subcarrier QPSK optical communication systems for different $\sigma_x$ for log-normal turbulence channel	52
Fig. 5.15 Comparison of BER performance of subcarrier BPSK and subcarrier QPSK optical communication systems for different SI for log-normal turbulence channel	52
Fig. 5.16 Minimum SNR required for maintaining BER of $10^{-6}$ for QPSK modulation scheme for log-normal turbulence channel	53
Fig. 5.17 Minimum SNR required for maintaining BER of $10^{-6}$ for different modulation scheme for log-normal turbulence channel	53
Fig. 5.18 BER performance of subcarrier BPSK optical communication systems for gamma-gamma turbulence channel	55
Fig. 5.19 BER performance of subcarrier QPSK optical communication systems for gamma-gamma turbulence channel	56
Fig. 5.20 Symbol-error probability, for $Q=2, M=N=1$ and no background noise, for log-normal channel with different S.I	57
Fig. 5.21 Symbol-error probability with varying $M$ , for $Q=2, N=1$ and no background noise, for log-normal channel with $\sigma_x = 0.6$	57

Fig. 5.22 Symbol-error probability for unfaded channel varying the bit rate, for a fixed background noise with $M=1$ and $N=1$ , for $Q=2$	58
Fig. 5.23 Symbol-error probability for log-normal fading ( $\sigma_x = 0.6$ ), varying the number of Tx. and Rx., with background noise $-170dBJ$	58
Fig. 5.24 Symbol-error probability with varying $M$ , for $Q=2, N=1$ and no background noise, for gamma-gamma channel with $S.I = 0.4$ and $S.I = 3.0$ .	59
Fig. 5.25 Symbol-error probability with varying $N$ , for $Q=2, M=1$ and no background noise, for gamma-gamma channel with $S.I = 0.4$ .	59
Fig. 5.26 Symbol-error probability for unfaded channel varying the bit rate, for a fixed background noise with $M=1$ and $N=1$ , for $Q=2$	60
Fig. 5.27 Symbol-error probability for gamma-gamma fading ( $S.I = 0.4$ ), varying the number of Tx. and Rx., with background noise $-170dBJ$ .	60

# List of Tables

Table 1.1 Comparison of wireless Optical and Communicational Channel	2
Table 2.1 Comparison of wireless optical topologies	14
Table 2.2 Interpretation of IEC safety classification for optical sources	16
Table 2.3 Point source safety classification based on allowable average optical power output for a variety of optical wavelengths	17
Table 5.1 System Parameters	42



## Abstract

Free space optical (FSO) communication technology is a promising candidate for next generation broadband networking, due to its large bandwidth potential, unlicensed spectrum, excellent security and quick and inexpensive setup and used to solve the “last mile” problem to bridge the gap between the end user and the fiber-optic infrastructure already in place [1, 2]. Its unique properties make it also appealing for a number of other applications, including metropolitan area network extensions, local area network connectivity, fiber backup, back-haul for wireless cellular networks, redundant link and disaster recovery. In FSO communications, optical transceivers communicate directly through the air to form point-to-point line-of-sight (LOS) links. One major impairment over FSO links is the atmospheric turbulence, which occurs as a result of the variations in the refractive index due to inhomogeneities in temperature and pressure fluctuations [3, 4]. Atmospheric turbulence has been studied extensively and various theoretical models have been proposed to describe turbulence-induced image degradation and intensity fluctuations (i.e., signal fading) [5, 6]. Performance of single receiver system for log-normal model has already been studied [7]. But it is very important to consider other turbulence model as well as other modulation scheme.



# Chapter 1

## Introduction

### 1.1 General Perspective

In recent years, there has been a migration of computing power from the desktop to portable, mobile formats. Devices such as digital still and video cameras, portable digital assistants and laptop computers offer users the ability to process and capture vast quantities of data. Although convenient, the interchange of data between such devices remains a challenge due to their small size, portability and low cost. High performance links are necessary to allow data exchange from these portable devices to established computing infrastructure such as backbone networks, data storage devices and user interface peripherals [8]. For this purpose, some parts of communication links need to be constructed wireless. During the last decade, therefore, the wireless communication technology has grown rapidly [9] - [12]. The technology base for implementing this concept does not yet exist, however. Radio technology, although well-suited for moderate-speed applications such as voice, may not be sufficient to support many high-speed applications.

Table 1.1: Comparison of wireless Optical and Communicational Channel

Property	Wireless Optical	Radio
RF circuit design	No	Yes
Bandwidth regulated	No	Yes
Data rate	100's Mbps	10's Mbps
Security	High	Low

## 1.2 Brief History of Optical Wireless Communication

In early 1790s, Claude Chappe invented the optical telegraph which was able to send messages over distances by changing the orientation of signalling arms on a large tower. A code book of orientations of the signalling arms was developed to encode letters of the alphabet, numerals, common words and control signals. Messages could be sent over distances of hundreds of kilometers in a matter of minutes [23]. One of the earliest wireless optical communication devices using electronic detectors was the photophone invented by A. G. Bell and C. S. Tainter and patented on December 14, 1880 . The system is designed to transmit a operators voice over a distance by modulating reflected light from the sun on a foil diaphragm. The receiver consisted of a selenium crystal which converted the optical signal into an electrical current. With this setup, they were able to transmit an audible signal a distance of 213 m [24].

Optical transmission came to be available for the communication system after the laser as a light source was invented. As a coherent light source being not in a nature, ruby laser was invented by Dr. T. Mainman in 1960, He-Ne laser oscilated in Bel Labs next year, and GaAs semiconductor laser oscillated in 1962. The continuous oscillation of GaAlAs laser was realized in Japan, the United States and the Soviet Union in 1970, and the small semiconductor laser which could be high-speed modulated advanced optical transmission technology greatly. Around from 1965, the beam guide system which arranged the lens in a pipe, and the space propagation system which emits light to free space were beginning to be studied so as to use laser for free space optical communication. In 1979, indoor optical wireless communication system has been presented by F. R. Gfeller and U. Bapst [25]. In their system, diffuse optical radiation in the near-infrared region was utilized as signal carrier to interconnect a cluster of terminals located in the same room to a common cluster controller. However, the reduction in loss of the fiber and the invention of continuous semiconductor laser has moved the mainstream of the research to optical fiber transmission, and the utilization of optical transmission system was accelerated from 1970 to 1980.



## 1.3 Objective of The Thesis

The objective of the research work are:

- To carry out theoretical analysis of a free space optical link over scintillation channel to find the comparison of bit error rate (BER) with on-off keying (OOK), Q-ary pulse position modulation (PPM) and subcarrier modulation schemes.
- To evaluate the BER performance results for difficult atmospheric condition.
- To extend the analytical model to spatial diversity scheme and to find the performance improvement due to diversity.

## 1.4 Organization of This Thesis

This thesis consists of seven chapters. Chapter 1 discusses the purposes and position of this study, and importance of optical wireless communication in communication field in recent years, and the main objective if this work.

In Chapter 2, a brief overview of different components and different terminologies used in FSO communication is discussed.

In Chapter 3, two popular channel model log-normal and gamma-gamma turbulence model are presented which are extensively used in wireless communication. Log-normal channel model is normally used in weak turbulence condition and gamma-gamma model is best suited for moderate and strong turbulence condition.

In Chapter 4, optical OOK is extensively analyzed for different condition. In the next part of the chapter we analyzed BER performance of FSO link employing subcarrier PSK for different turbulence condition and different turbulence model. Then optical Q-ary PPM is extensively analyzed for different condition and different turbulence model.

In Chapter 5, simulate performance result are presented for different conditions which are theoretically analyzed in chapter 4.

Finally, some conclusions and suggestions for future work are provided in Chapter 6.

## **Chapter 2**

# **Basic Knowledge of Optical Wireless Communication Systems**

### **2.1 Introduction**

This chapter introduces some basic concepts used in the following chapters which are required for the understanding of this work. We begin with the importance of free space optical communication in Section 2.2. A review of the brief description of major components of a optical wireless link comes next in Section 2.3. Section 2.4 describes the characteristics of different channel topologies and their relative advantage and disadvantage. Throughout the thesis point to point link is considered. Finally Section 2.5 gives the different safety considerations for free-space optical link because optical radiation can damage skin or eye of human being.

### **2.2 Importance of Free-Space Optical Communication in Communication System**

Communication systems transmit information from a transmitter to a receiver through the construction of a time-varying physical quantity or a signal. A familiar example of such a system is a wired electronic communications system in which information is conveyed from the transmitter by sending an electrical current or voltage signal through a conductor to a receiver circuit. Another example is wireless radio frequency (RF) communications in which a transmitter varies the amplitude, phase and frequency of an electromagnetic carrier which is detected by a receive antenna and electronics. In each of these communications systems, the transmitted signal is corrupted by deterministic and random distortions due

to the environment. For example, wired electrical communication systems are often corrupted by random thermal as well as shot noise and are often frequency selective. These distortions due to external factors are together referred to as the response of a communications channel between the transmitter and receiver. For the purposes of system design, the communications channel is often represented by a mathematical model which is realistic to the physical channel. The goal of communication system design is to develop signalling techniques which are able to transmit data reliably and at high rates over these distorting channels. As a medium for wireless communication, lightwave radiation offers several significant advantages over radio. Lightwave emitters and detectors capable of high speed operation are available at low cost. The lightwave spectral region offers a virtually unlimited bandwidth that is unregulated worldwide. Infrared and visible light are close together in wavelength, and they exhibit qualitatively similar behavior. Both are absorbed by dark objects, diffusely reflected by light-colored objects, and directionally reflected from shiny surfaces. Both types of light penetrate through glass, but not through walls or other opaque barriers, so that optical wireless transmissions are confined to the room in which they originate. This signal confinement makes it easy to secure transmissions against casual eavesdropping, and it prevents interference between links operating in different rooms. Thus, optical wireless networks can potentially achieve a very high aggregate capacity, and their design may be simplified, since transmissions in different rooms need not be coordinated. When an optical wireless link employs intensity modulation with direct detection (IM/DD), the short carrier wavelength and large-area square-law detector lead to efficient spatial diversity that prevents multi-path fading. By contrast, radio links are typically subject to large fluctuations in received signal magnitude and phase. Freedom from multi-path fading greatly simplifies the design of optical wireless links.

The lightwave is not without drawbacks however. Because lightwave cannot penetrate walls, communication from one room to another requires the installation of optical wireless access points that are interconnected via a wired backbone. In many applications, there exists intense ambient light noise, arising from sunlight, incandescent lighting and fluorescent lighting, which induce noise in an

optical wireless receiver. In virtually all short-range, indoor applications, IM/DD is the only practical transmission technique. The signal-to-noise ratio (SNR) of a direct detection receiver is proportional to the square of the received optical power, implying that IM/DD links can tolerate only a comparatively limited path loss. Often optical wireless link must employ relatively high transmit power levels and operate over a relatively limited range. While the transmitter power level can usually be increased without fear of interfering with other users, transmitter power may be limited by concerns of power consumption and eye safety, particularly in portable transmitters.

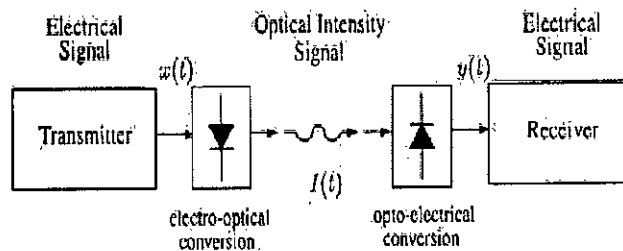


Fig. 2.1: Block diagram of optical intensity, direct detection communication channel.

## 2.3 Brief Description of Major Components of a Optical Wireless Link

An optical wireless links consists of a transmitter, wireless communication channels and a receiver as shown in Fig. 2.1.

### 2.3.1 Optical Sources

In most optical communication systems, semiconductor light sources are used to convert electrical signals into light. Optical sources for wireless transmission must be compatible to overcome the atmospheric effects and they should be such that one can easily modulate the light directly at high data rates. Generally either LASERs or LEDs are used in optical communication systems.

## **LED**

Light emitting diodes (LEDs) used in optical communication system are the same as visual display LEDs except that they operate in the infra-red region and with many times higher intensity of emission. When the p-n junction is forward biased, photon emission takes place due to recombination of electron-hole pair. The wavelength of emission will depend on the energy gap.

## **LASER**

Laser stands for "light amplification by stimulating emission of radiation". Compared to LED, a laser has wider bandwidth, higher power output, higher modulation efficiency, narrower spectral line-width and narrower emission pattern. Laser sources are much brighter than LEDs.

### **2.3.2 Optical Detectors**

An optical detector is a photon (light) to electron converter. Avalanche photodiode (APD) and positive intrinsic negative (PIN) diode are the most commonly used detectors. The most important thing of the optical communication system is that the spectral response of both the source and the detector must be same, otherwise efficiency will suffer.

#### **PIN**

PIN is the simplest optical detector. It is composed of an n+ substrate, a lightly doped intrinsic region and a thin p zone. Operated with a reverse bias, mobile carriers leave the p-n junction producing a zone of moderate electric field on both sides of the junction into the intrinsic region. As it only lightly doped, this field extends deeply. Incident light power is mainly absorbed in the intrinsic region, causing electron hole pairs to be generated. These carriers are separated by the influence of the electric field in the intrinsic region and represent a reverse diode current that can be amplified.

#### **APD**

It is the second popular type of photodetector and has the advantage of internally multiplying the primary detected photocurrent by avalanche process, thus

increasing the signal detection sensitivity. But some noises are also generated here.

The frequency response of both PIN and APD are similar, making them both suitable up to 1 GHz. The main advantage of APD over PIN diode is greater gain bandwidth product due to the inbuilt gain. Silica is the material used at short wavelength ( $< 1\mu m$ ), GE, InGaAsP and AlGaAsP becoming popular at the longer wavelength around 1.3  $\mu m$ .

## 2.4 Channel Topologies

The characteristics of the wireless optical channel can vary significantly depending on the topology of the link considered. This section presents three popular wireless optical channel topologies and discusses the channel characteristics of each.

### 2.4.1 Point-to-point Links

Point-to-point wireless optical links operate when there is a direct unobstructed path between a transmitter and a receiver. Figure 2.2 presents a diagram of a typical point-to-point wireless optical link. A link is established when the transmitter is oriented toward the receiver. In narrow field-of-view applications this oriented configuration allows the receiver to reject ambient light and achieve high data rates and low path loss. The main disadvantage of this link topology is that it requires pointing and is sensitive to blocking and shadowing. The frequency response of these links is limited primarily by front-end photodiode capacitance. Since inexpensive large-area photodiodes are typically used with limited reverse bias the depletion capacitance significantly limits the link bandwidth [8].

A typical example of these links is the standard Infrared Data Association (IrDA) Fast IR 4Mbps link. These links offer communication over 1m of separation and are used primarily for data interchange between portable devices. The achievable bandwidth in these inexpensive systems is on the order of 10–12MHz which is approximately three orders of magnitude smaller than in wired fibre-optic systems. New IrDA point-to-point links operating at 16Mbps have also been standardized and may begin appearing in a wider range of applications. Another

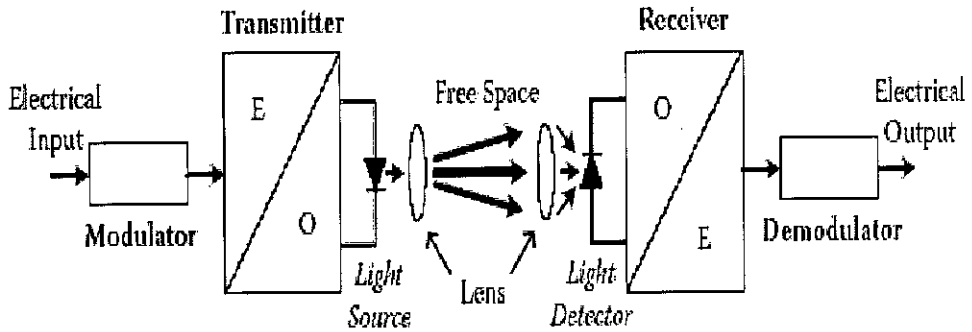


Fig. 2.2: Block diagram of point to point optical link

channel topology which uses a number of parallel point-to-point links is the space division multiplexing architecture. Space division multiplexing is a technique by which a transmitter outputs different data in different spatial directions to allow for the simultaneous use of one wavelength by multiple users. In one such system a ceiling-mounted base station has a number of narrow beams establishing point-to-point links in a variety of directions in a room. A fixed receiver once aligned to within 1 of a transmitter beam establishes a high speed link at up to  $50\text{Mb/s}$ . Another means of implementing a space division multiplexing system is to use a tracked optical wireless architecture. In this system the transmitter beams are steerable under the control of a tracking subsystem. Tracking is typically accomplished by a beacon LED or FM transmitter on the mobile terminal. These systems are proposed to provide  $155\text{Mb/s}$  ATM access to mobile terminals in a room. Electronic tracking systems have also been proposed which exploit a diffuse optical channel to aid in acquisition. The advantage of this topology is that it is extremely power efficient and supports a large aggregate bandwidth inside of a room at the expense of system complexity. Point-to-point wireless optical links have been implemented in a wide variety of short- and long-range applications. Short range infrared band links are being designed to allow for the transfer of financial data between a PDA or cellphone and a point-of-sale terminal. Wireless optical links are chosen as the transmission medium due to the low cost of the transceivers and the security available by confining optical radiation. The IrDA has specified a standard for this financial application under the title IrDAFM (financial messaging). Medium range indoor links have also been de-



veloped to extend the range of Ethernet networks in an office environment. A 10 Mbps point-to-point wireless infrared link to extend Ethernet networks has been deployed over a range of at most 10m. Higher rate 100Mbps point-to-point wireless infrared links have also been designed to extend Ethernet networks in indoor environments.

### 2.4.2 Diffuse Links

Diffuse transmitters radiate optical power over a wide solid angle in order to ease the pointing and shadowing problems of point-to-point links. Figure 2.10 presents a block diagram of a diffuse wireless optical system. The transmitter does not need to be aimed at the receiver since the radiant optical power is assumed to reflect from the surfaces of the room. This affords user terminals a wide degree of mobility at the expense of a high path loss. These channels however suffer not only from optoelectronic bandwidth constraints but also from low-pass multipath distortion [13]. Unlike radio frequency wireless channels diffuse channels do not exhibit fading. This is due to the fact that the receive photodiode integrates the optical intensity field over an area of millions of square wavelengths and hence no change in the channel response is noted if the photodiode is moved a distance on the order of a wavelength [14]. Thus the large size of the photodiode relative to the wavelength of light provides a degree of spatial diversity which eliminates multipath fading. Multipath distortion gives rise to a channel bandwidth limit of approximately 10-200 MHz depending on room layout shadowing and link configuration [14, 15]. Many channel models based on measurements allow for the accurate simulation of the low-pass frequency response of the channel . The IrDA and the IEEE have similar standards for diffuse infrared links. The IrDA Advanced Infrared (AIr) standard allows communication at rates up to 4 Mbps with repetition coding . The IEEE wireless infrared standard falls under the 802.11 standard and allows diffuse transmission at a maximum of 2 Mbps . Both systems used pulse-position modulation (PPM) which is a coded version of on-off keying. Experimental indoor wireless optical links have been demonstrated at 50 Mbps using on-off keying over a horizontal range of approximately 3 m . A commercial indoor diffuse wireless optical link aimed at digital audio and set-top box applications claims data rates of up to 5 Mbps in typical indoor environments

. An early diffuse wireless optical system was employed in a portable computer called PARCTAB, developed at the Xerox Palo Alto Research Center (PARC) in 1993 . The diffuse link was able to provide data rates of up to 19.2 kbps and was used to communicate electronic mail and other data to a hand-held computing device.

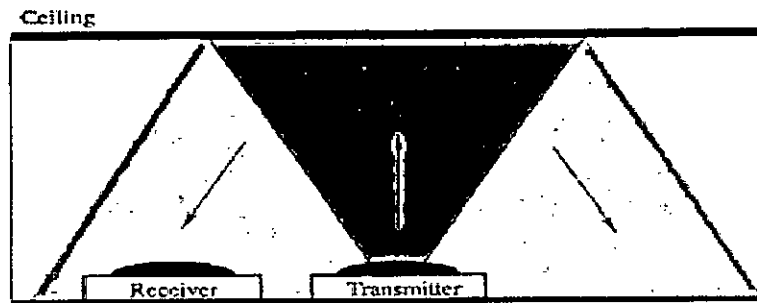


Fig. 2.3: A diffuse optical wireless communication system

### 2.4.3 Quasi-Diffuse Links

The transmitter illuminates the ceiling with a series of slowly diverging beam sources which illuminate a grid of spots on the ceiling. In experimental settings these multiple beams are created using individual light sources [18] and proposed techniques using holographic beam splitters appear promising [19]. The transmit beams suffer a small path loss nearly independent of the length of the link from the transmitter to the ceiling due to the low beam divergence. The data transmitted on all beams is identical. The receiver consists of multiple concentrator/photodiode pairs each with a non-overlapping narrow FOV of the ceiling. The FOV of each receiver is typically set to see at least one spot on the ceiling. These narrow FOV receivers reject a majority of multipath distortion and provide a link with an improved bandwidth although the link is more sensitive to shadowing relative to diffuse links. Spatially localized interferers such as room illumination can be rejected by using the spatial diversity of the multiple receivers. In a diffuse scheme all the noise power is collected along with the signal power.

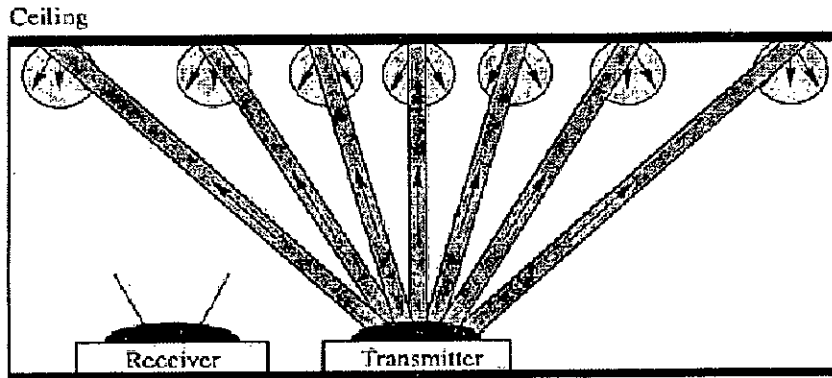


Fig. 2.4: A quasi-diffuse optical wireless communication system

Table 2.1: Comparison of wireless optical topologies

	point to point	diffuse	quasi-diffuse
Rate	High	Low-Moderate	Moderate
Pointing Required	Yes	No	Somewhat
Immunity to Blocking	Low	High	Moderate-High
Mobility	Low	High	Moderate-High
Complexity of Optics	Low	Low-Moderate	High
Ambient Light Rejection	High	Low	High
Multipath Distortion	None	High	Low
Path Loss	Low	High	Moderate

#### 2.4.4 Comparison of Different Technologies

Table 2.1 presents a comparison of some of the characteristics of the three channel topologies discussed. The point-to-point topology is a low complexity means to achieve high data rate links at the expense of mobility and pointing requirements. Diffuse links suffer from high path loss but offer a great degree of mobility and robustness to blocking. Quasi-diffuse links permit higher data rates by requiring users to aim their receivers at the ceiling but suffer from a higher implementation cost due to the multi-beam transmitter. Thus each channel topology is suited to a different application depending on required data rates and channel conditions. It may also be advantageous to combine the operation of the various topologies to form a more robust link. Recent work has demonstrated experimental configurations which use a diffuse wireless optical channel to aid in acquiring tracking and to serve as a backup link to improve user mobility [20].

## 2.5 Eye and Skin Safety

Safety considerations must be taken into account when designing a wireless optical link. Since the energy is propagated in a free-space channel, the impact of this radiation on human safety must be considered. There are a number of international standards bodies which provide guidelines on LED and laser emissions namely: the International Electrotechnical Commission (IEC) (IEC60825-1), American National Standards Institute (ANSI) (ANSI Z136.1), European Committee for Electrotechnical Standardization (CENELEC) among others. In this section, we will consider the IEC standard which has been widely adopted. This standard classifies the main exposure limits of optical sources. Table 2.2 includes a list of the primary classes under which an optical radiator can fall. Class 1 operation is most desirable for a wireless optical system since emissions from products are safe under all circumstances. Under these conditions, no warning labels need to be applied and the device can be used without special safety precautions. This is important since these optical links are destined to be inexpensive, portable and convenient for the user. An extension to Class 1, termed Class 1M, refers to sources which are safe under normal operation but which may be hazardous if viewed with optical instruments [16]. Longer distance free-space links often operate in class 3B mode, and are used for high data rate transmission over moderate distances (40 m). The safety of these systems is maintained by locating optical beams on rooftops or on towers to prevent inadvertent interruption [17]. On some longer range links, even though the laser emitter is Class 3B, the system can still be considered Class 1M if appropriate optics are employed to spread the beam over a wide enough angle.

The choice of which optical wavelength to use for the wireless optical link also impacts the AEL. Table 2.3 presents the limits for the average transmitted optical power for the IEC classes listed in Table 2.2 at four different wavelengths. The allowable average optical power is calculated assuming that the source is a point emitter, in which the radiation is emitted from a small aperture and diverges slowly as is the case in laser diodes. Wavelengths in the 650 nm range are visible red light emitters. There is a natural aversion response to high intensity sources in the visible band which is not present in the longer wavelength infrared

Table 2.2: Interpretation of IEC safety classification for optical sources

Safety class	Interpretation
Class 1	Safe under reasonably foreseeable conditions of operation
Class 2	Eye protection afforded by aversion responses including blink reflex.
Class 3A	Safe for viewing with unaided eye. Direct intra-beam viewing with optical aids may be hazardous.
Class 3B	Direct intra-beam viewing is always hazardous. Viewing diffuse reflections in normally safe.

band. The visible band has been used rarely in wireless optical communication applications due to the high background ambient light noise present in the channel. However, there has been some development of visible band wireless optical communications for low-rate signalling . Infrared wavelengths are typically used in optical networks. The safety of these systems is maintained by locating optical beams on rooftops or on towers to prevent inadvertent interruption . On some longer range links, even though the laser emitter is Class 3B, the system can still be considered Class 1M if appropriate optics are employed to spread the beam over a wide enough angle.

The critical parameter which determines whether a source falls into a given class depends on the application. The allowable exposure limit (AEL) depends on the wavelength of the optical source, the geometry of the emitter and the intensity of the source. In general, constraints are placed on both the peak and average optical power emitted by a source. For most practical high frequency modulated sources, the average transmitted power of modulation scheme is more restrictive than the peak power limitation and sets the AEL for a given geometry and wavelength [12]. At modulation frequencies greater than about 24 kHz, the AEL can be calculated based on average output power of the source [13].

Eye safety considerations limit the average optical power which can be transmitted. This is another fundamental limit on the performance of free-space optical links.

Table 2.3: Point source safety classification based on allowable average optical power output for a variety of optical wavelengths

Safety Class	650nm visible	880 nm infrared	1310 nm infrared	1550 nm infrared
Class 1	<0.2mW	<0.5mW	<8.8mW	<10mW
Class 2	<0.2-1mW	n/a	n/a	n/a
Class 3A	1-5mW	0.5-2.5mW	8.8-45mW	10-50mW
Class 3B	5-500mW	2.5-500mW	45-500mW	50-500mW

## Chapter 3

# Distribution Models for Turbulence-Induced Intensity Fading

In this section, we review each of the two channel models used throughout the thesis and discuss their relations among them.

### 3.1 Log-normal pdf

#### 3.1.1 Marginal Distribution of Fading

For propagation distances less than a few kilometers, variations of the log-amplitude are typically much smaller than variations of the phase. Over longer propagation distances, where turbulence becomes more severe, the variation of the log-amplitude can become comparable to that of the phase. Based on the atmosphere turbulence model adopted here and assuming weak turbulence, we can obtain the approximate analytic expression for the covariance of the log-amplitude fluctuation of plane and spherical waves which is also known as Rytov variance [27]:

$$\sigma_X^2|_{plane} = 0.56 \left( \frac{2\pi}{\lambda} \right) \int_0^L C_n^2(x) (L-x)^{5/6} dx \quad (3.1)$$

$$\sigma_X^2|_{spherical} = 0.56 \left( \frac{2\pi}{\lambda} \right) \int_0^L C_n^2(x) \left( \frac{x}{L} \right) (L-x)^{5/6} dx \quad (3.2)$$

where  $C_n^2(z)$  is the wavenumber spectrum structure parameter, which is altitude-

dependent. Hufnagel and Stanley gave a simple model for  $C_n^2(z)$  [28]:

$$C_n^2(z) = K_o z^{-1/3} \exp\left(\frac{-z}{z_o}\right) \quad (3.3)$$

where  $K_o$  is parameter describing the strength of the turbulence and  $z_o$  is the effective height of the turbulent atmosphere. For atmospheric channels near the ground ( $z < 18.5m$ ),  $C_n^2$  can vary from  $10^{-13}m^{-2/3}$  for strong turbulence  $10^{-17}m^{-2/3}$  to for weak turbulence, with  $10^{-15}m^{-2/3}$  often quoted as a typical average value [3]. Note that in Eq. 3.3,  $C_n^2$  is influenced by many physical factors, including altitude, surrounding terrain and weather conditions (temperature, humidity, wind strength and direction).

As the Rytov variance increases, the scintillation index continues to increase beyond the weak turbulence regime until it reaches a maximum value greater than unity. At that point the scintillation index begins to decrease with increasing Rytov variance and approaches unity from above. This region is termed the saturation region. Since the measured scintillation index is greater than unity, this implies the system is neither operating in the weak or saturation regions, but somewhere in between the two extremes - i.e. moderate turbulence conditions. The distribution of the irradiance fluctuations is dependent on the strength of the optical turbulence. For the weak turbulence regime, the fluctuations are generally considered to be lognormal distributed, and for very strong turbulence, exponentially distributed. For moderate turbulence, the distribution of the fluctuations is not well understood, and a number of distributions have been proposed (such as the Beckmann distribution [21], K-distribution [22] and Gamma- Gamma distribution).

Consider the propagation of light through a large number of elements of the atmosphere, each causing an independent, identically distributed phase delay and scattering. By the Central Limit Theorem, the marginal distribution of the log-amplitude is Gaussian:

$$f_X(X) = \frac{1}{(2\pi\sigma_X^2)^{1/2}} \exp\left\{-\frac{(X - E[X])^2}{2\sigma_X^2}\right\} \quad (3.4)$$

The light intensity  $I$  is related to the log-amplitude  $X$  by



$$I = I_0 \exp(2X - E[X]) \quad (3.5)$$

Where  $E[X]$  is the ensemble average of log-amplitude  $X$ . From 3.4 and 3.5, the average light intensity is:

$$E[I] = E[I_0 \exp(2X - 2E[X])] = I_0 \exp(2\sigma_x^2) \quad (3.6)$$

Hence, the marginal distribution of light intensity fading induced by turbulence is log-normal:

$$f_I(I) = \frac{1}{2I} \frac{1}{(2\pi\sigma_x^2)^{1/2}} \exp\left\{-\frac{[\ln(I) - \ln(I_0)]^2}{8\sigma_x^2}\right\} \quad (3.7)$$

In the log normal model the amplitude of the random path gain  $A$  can be written as  $A = e^X$ . The scintillation index (S.I.), a measure of the strength of atmospheric fading, known to information theorists as the amount of fading [29], is defined as

$$S.I. = \frac{E[A^4]}{E^2[A^2]} - 1 \quad (3.8)$$

which, for this distribution, can be shown to equal  $S.I. = e^{4\sigma_x^2} - 1$ . Typical values appearing in the literature are S.I. in the range of 0.4 – 1.0.

Rayleigh fading emerges from a scattering model that views the composite field as produced by a large number of nondominating scatterers, each contributing random optical phase upon arrival at the detector. We again normalize so that  $E^2[A^2] = 1$ , giving  $S.I. = 1$  for the Rayleigh case, though the distribution is quite different from the log-normal case, especially in the small-amplitude tail.

### 3.1.2 Joint Spatial and Temporal Distributions of Fading

We assume that the log-amplitude at  $n$  receivers is described by a joint Gaussian distribution. The auto-covariance matrix of the log-amplitude at  $n$  receivers in a

plane transverse to the direction of propagation is given by [40]

$$C_X = \begin{bmatrix} \sigma_X^2 & \sigma_X^2 b_X(d_{12}) & \cdots & \sigma_X^2 b_X(d_{1n}) \\ \sigma_X^2 b_X(d_{21}) & \sigma_X^2 & \cdot & \sigma_X^2 b_X(d_{2n}) \\ \cdots & \cdots & \cdots & \cdots \\ \sigma_X^2 b_X(d_{n1}) & \sigma_X^2 b_X(d_{2n}) & \cdots & \sigma_X^2 \end{bmatrix}_{n \times m} \quad (3.9)$$

where  $d_{ij}$  is the distance between points  $i$  and  $j$  in the receiver plane. Based on frozenin model, and ignoring wind velocity fluctuations, Eq. 3.9 can also be modified to describe temporal fading correlation by making the substitution

$$d_{ij} = |i - j|Tu_{\perp} \quad (3.10)$$

where  $T$  is the time interval between observations. In all that follows, we assume a communication system using OOK, in which case,  $T$  is the bit interval. We denote the covariance matrix of a string of  $n$  bits as

$$C_X^T = \begin{bmatrix} \sigma_X^2 & \sigma_X^2 b_X(\frac{T}{\tau_0} d_0) & \cdots & \sigma_X^2 b_X(\frac{(n-1)T}{\tau_0} d_0) \\ \sigma_X^2 b_X(\frac{T}{\tau_0} d_0) & \sigma_X^2 & \cdot & \sigma_X^2 b_X(\frac{(n-2)T}{\tau_0} d_0) \\ \cdots & \cdots & \cdots & \cdots \\ \sigma_X^2 b_X(\frac{(n-1)T}{\tau_0} d_0) & \sigma_X^2 b_X(\frac{(n-2)T}{\tau_0} d_0) & \cdots & \sigma_X^2 \end{bmatrix}_{n \times m} \quad (3.11)$$

## 3.2 Gamma-gamma Distribution

Under weak fluctuation conditions, the scintillation index [Eq.(3.8)] increases with increasing values of the Rytov variance [Eq.(3.2)]. The scintillation index continues to increase beyond the weak fluctuation regime and reaches a maximum value greater than unity (sometimes as large as 5 or 6) in the regime characterized by random focusing [30]. With increasing path length or inhomogeneity strength, the focusing effect is weakened by multiple self-interference and the fluctuations slowly begin to decrease, saturating at a level for which the scintillation index approaches unity from above.

In a recent series of papers on scintillation theory, the irradiance of the received optical wave is modeled as a product  $I = I_x I_y$ , where  $I_x$  arises from large-scale turbulent eddies and  $I_y$  from small scale eddies. It is assumed that  $I_x$  and  $I_y$  are statically independent random processes for which the second moment of

irradiance is

$$\langle I^2 \rangle = \langle I_x^2 \rangle \langle I_y^2 \rangle \quad (3.12)$$

It is assumed that both large-scale and small-scale irradiance fluctuations are governed by gamma distributions, namely

$$f_{I_x}(I_x) = \frac{\alpha (\alpha I_x)^{\alpha-1}}{\Gamma \alpha} \exp(-\alpha I_x), \quad I_x > 0, \quad \alpha > 0; \quad (3.13)$$

$$f_{I_y}(I_y) = \frac{\beta (\beta I_y)^{\beta-1}}{\Gamma \beta} \exp(-\beta I_y), \quad I_y > 0, \quad \beta > 0; \quad (3.14)$$

By first fixing  $I_x$  and writing  $I_y = I/I_x$ , we obtain the conditional pdf

$$f_{I_y}(I/I_x) = \frac{\beta (\beta I/I_x)^{\beta-1}}{\Gamma \beta} \exp(-\beta I/I_x), \quad I > 0, \quad (3.15)$$

To obtain the unconditional irradiance distribution, we form the average of Eq. 3.15 over the gamma distribution of Eq. 3.13

$$f(I) = \frac{2(\alpha\beta)^{(\alpha+\beta)/2}}{\Gamma(\alpha)\Gamma(\beta)} I^{\frac{\alpha+\beta}{2}-1} K_{\alpha-\beta}(2\sqrt{\alpha\beta I}), I > 0 \quad (3.16)$$

where  $K_a(\cdot)$  is the modified Bessel function of the second kind of order  $a$ . Here,  $\alpha$  and  $\beta$  are the effective number of small-scale and large scale eddies of the scattering environment. These parameters can be directly related to atmospheric conditions according to [31]

$$\alpha = \left[ \exp \left( \frac{0.49\sigma_X^2}{\left(1 + 1.11\sigma_X^{12/5}\right)^{(7/6)}} \right) - 1 \right]^{-1} \quad (3.17)$$

$$\beta = \left[ \exp \left( \frac{0.51\sigma_X^2}{\left(1 + 0.69\sigma_X^{12/5}\right)^{(7/6)}} \right) - 1 \right]^{-1} \quad (3.18)$$

### 3.3 Comparison

Fig. 3.1 shows the standard deviation of the log-amplitude fluctuation  $\sigma_X$  for a plane wave, computed using (3.2). In Fig. 3.1 we again assume a wavelength of

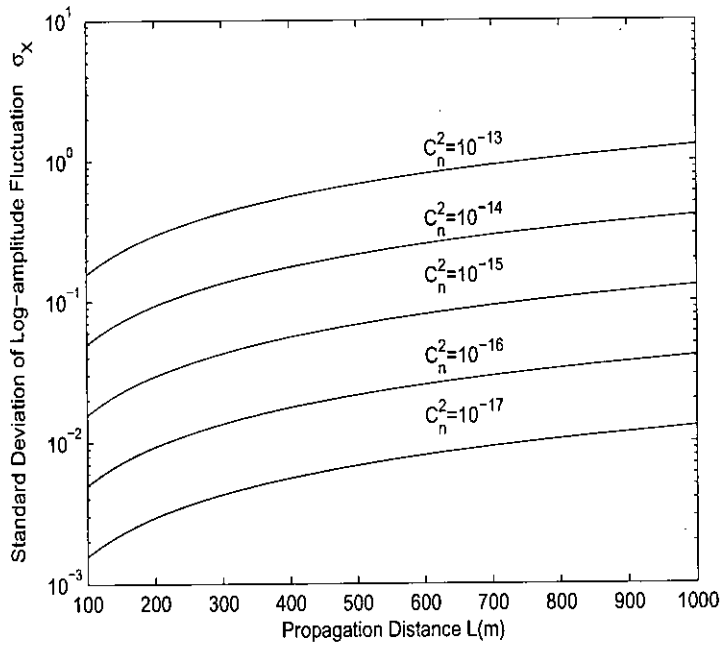


Fig. 3.1: Standard deviation of the log-amplitude fluctuation versus propagation distance for a plane wave.

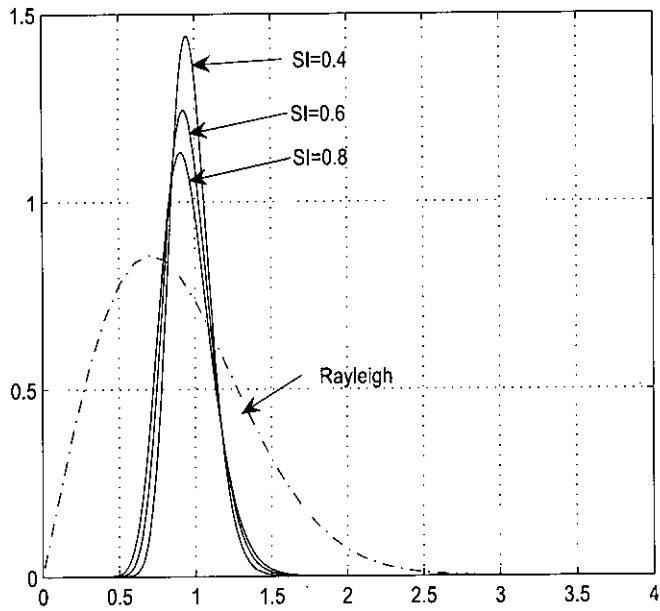


Fig. 3.2: Log-normal and Rayleigh pdfs

1550 nm and assume  $C_n^2(z)$  to be constant.

Fig. 3.2 shows probability density functions (pdfs) for the Rayleigh and log-normal cases with two typical values of S.I. In particular, notice the Rayleigh model has a much higher density in the low amplitude region, leading to a more severe impact on system performance.

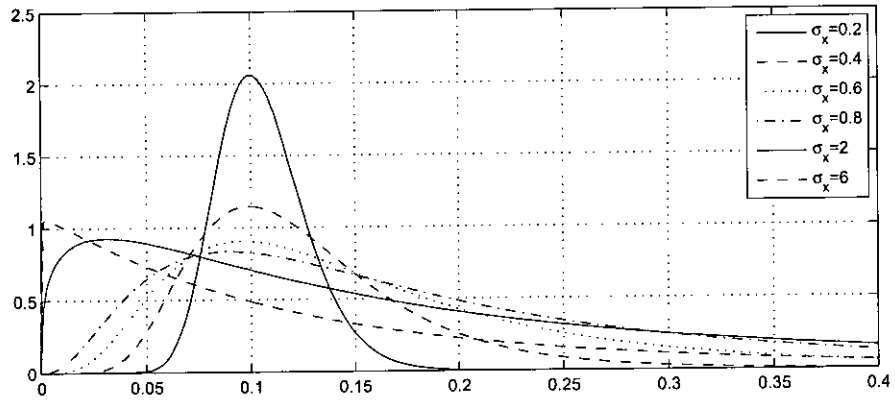


Fig. 3.3: Distribution of intensity fluctuations for several values of the turbulence strength

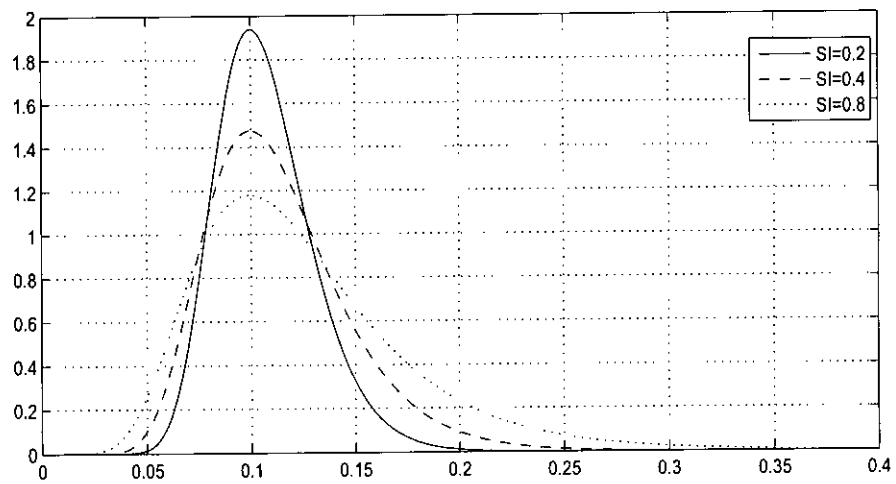


Fig. 3.4: Distribution of intensity fluctuations for several values of the S.I

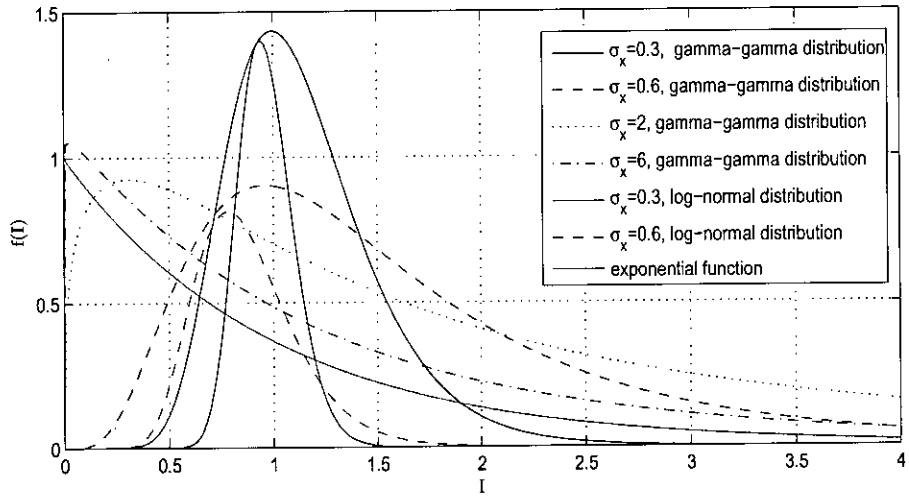


Fig. 3.5: Distribution of intensity fluctuations for different models

The gamma-gamma model approaches for heavy turbulence the exponential distribution, whereas in less turbulence it is suitable approximated by a log-normal distribution.

# Chapter 4

## Performance Analysis

### 4.1 Introduction

At first we describe the free-space optical communication system through block diagram in Section 4.2. In Section 4.3, theoretical analysis is presented for evaluating the performance of a log-normal channel using OOK. In this section, we also derived the expression for spatial diversity reception. In Section 4.4 theoretical analysis are carried out for both log-normal and gamma-gamma channel employing subcarrier BPSK and QPSK. In the next Section 4.5 theoretical analysis is derived for Q-ary PPM modulation system for both log-normal and gamma-gamma channel.

### 4.2 Block Diagram of the Free-space Optical Communication System

Fig. 4.1 shows the block diagram of an optical communication system through the atmosphere. The information generated by a source is encoded by an encoder, interleaved, and modulated into an electrical waveform by an electrical modulator. In the optical modulator, the intensity of a light source is modulated by the output signal of the electrical modulator. The light source is a laser, characterized by its wavelength, power, and beam divergence angle. There is a collimator or telescope in the transmitter to determine the direction and the size of the laser beam. The receiver consists of an optical front end, a photo-detector, a demodulator, a deinterleaver, and a decoder. The optical front end contains lenses focusing the received optical field onto a photodetector. The photo-detector

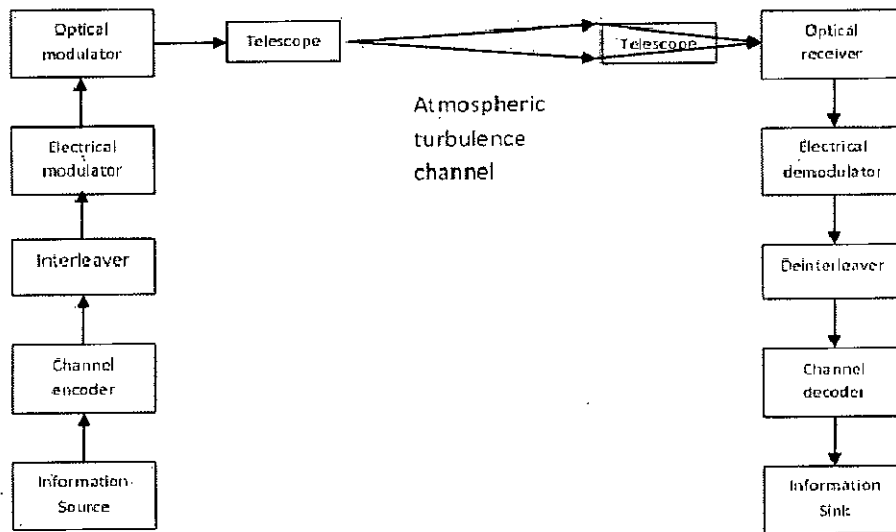


Fig. 4.1: Block Diagram of an Optical Communication System Through Atmospheric Turbulence Channel

converts the received optical field to an electronic signal, which is demodulated. The demodulator output signal is deinterleaved and decoded. The decoded bits are fed into an information sink.

## 4.3 Performance Analysis for OOK for Log-normal Turbulence Condition

### 4.3.1 System Model for OOK

In this thesis, we consider intensity modulation/direct detection (IM/DD) links using on-off keying (OOK). In most practical systems, the receiver signal-to-noise ratio (SNR) is limited by shot noise caused by ambient light much stronger than the desired signal and/or by thermal noise in the electronics following the photodetector. In this case, the noise can usually be modeled to high accuracy as additive, white Gaussian noise that is statistically independent of the desired signal. Let  $T$  denote the bit interval of the OOK system and assume that the receiver integrates the received photocurrent for an interval  $t_0 \leq T$  during each bit interval. At the end of the integration interval, the resulting electrical signal can be expressed as



$$r_e = \eta(I_s + I_b) + n \quad (4.1)$$

where  $I_s$  is the received signal light intensity and  $I_b$  is the ambient light intensity. Both of these quantities can be assumed to be constant during the integration time. The optical-to-electrical conversion coefficient is given by

$$\eta = \gamma T_o \cdot \frac{e\lambda}{hc} \quad (4.2)$$

where  $\gamma$  is the quantum efficiency of the photo-detector,  $e$  is the electron charge,  $\lambda$  is the signal wavelength,  $h$  is Planks constant,  $c$  is the speed of light. The additive noise  $n$  is white and Gaussian and has zero mean and covariance  $N/2$ , independent of whether the received bit is Off or On.

### 4.3.2 Performance Analysis for Log-normal Turbulence Channel

We assume that the receiver has knowledge of the marginal distribution of the turbulence-induced fading, but has no knowledge of the channels instantaneous fading. After subtraction of the ambient light bias  $\eta I_b$ , the signal  $r = r_e - \eta I_b$  is described by the following conditional densities when the transmitted bit is Off or On, respectively

$$P(r|Off) = \frac{1}{\sqrt{\pi N}} \exp\left(-\frac{r^2}{N}\right) \quad (4.3)$$

$$\begin{aligned} P(r|On) &= \int_{-\infty}^{\infty} P(r|On, X) f_X(X) dX \\ &= \int_{-\infty}^{\infty} \frac{1}{\sqrt{\pi N}} f_X(X) \\ &\quad \cdot \exp\left[-\frac{(r - \eta I_o e^{2X - 2E[X]})^2}{N}\right] dX \\ &= \int_{-\infty}^{\infty} \frac{1}{\sqrt{\pi N}} \frac{1}{(2\pi\sigma_X^2)^{1/2}} \exp\left\{-\frac{(X - E[X])^2}{2\sigma_X^2}\right\} \\ &\quad \cdot \exp\left[-\frac{(r - \eta I_o e^{2X - 2E[X]})^2}{N}\right] dX \end{aligned} \quad (4.4)$$

Let, the threshold be  $T_{th}$

$$T_{th}(r) = \frac{P(r|On)}{P(r|Off)} \quad (4.5)$$

The bit-error probability of OOK can be computed as:

$$P_b = P(Off) \cdot P(Bit\ Error|Off) + P(On) \cdot P(Bit\ Error|On) \quad (4.6)$$

Where  $P(Bit\ Error|Off)$  and  $P(Bit\ Error|On)$  denote the bit-error probabilities when the transmitted bit is Off and On, respectively. Without considering inter symbol interference, which can be ignored when the bit rate is not high and multi-path effects are not pronounced, we have

$$P(Bit\ Error|Off) = \int_{T_{th}(r)>1} P(r|Off)dr \quad (4.7)$$

$$P(Bit\ Error|On) = \int_{T_{th}(r)<1} P(r|On)dr \quad (4.8)$$

### 4.3.3 Performance Analysis for Log-normal Turbulence Channel in Spatial Diversity Reception

Spatial diversity reception, which has been well-studied for application at radio and microwave frequencies, has the potential to mitigate the degradation caused by atmospheric turbulence [32],[41]. Spatial diversity reception in free-space optical communication has been proposed and studied in [41]. In the EGC scheme, we assume that the receiving party has knowledge of the marginal distribution of the fading at each receiver, but has no knowledge of the fading correlation or the instantaneous fading state. For each individual receiver output, we can find an optimum threshold  $T_i$ . The EGC detector then adds together the n receiver outputs with equal gains and compares the sum to the threshold:

$$T_{th} = \sum_{i=1}^n T_i \quad (4.9)$$

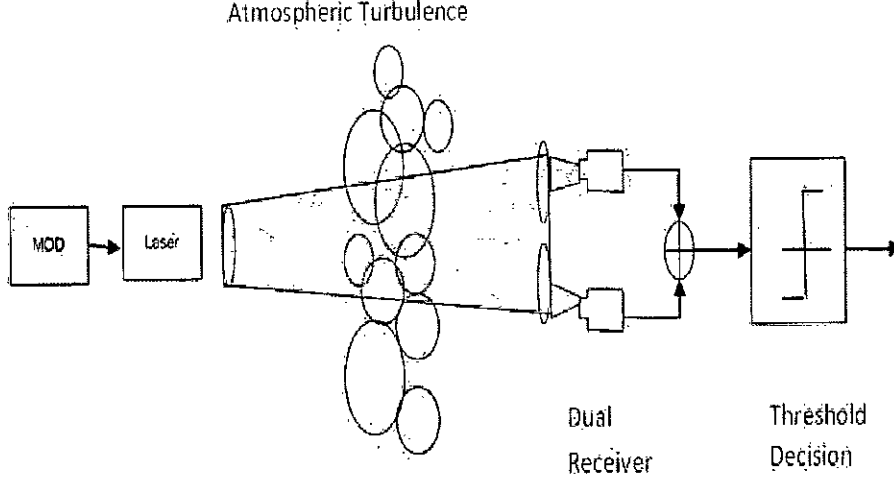


Fig. 4.2: Dual branch reception on atmospheric turbulence channels with correlated turbulence-induced fading equal-gain combining with threshold detection

The error probability of EGC is

$$P_b = \int_{\vec{X}} f_{\vec{X}} P(\text{BitError}|\vec{X}) d\vec{X} \quad (4.10)$$

where

$$P(\text{BitError}|\vec{X}) = P(\text{Off}) \cdot Q\left(\frac{T_{th}}{\sqrt{2N}}\right) + P(\text{On}) \cdot Q\left[\frac{\eta I_o(e^{2X_1-2E[X_1]} + e^{2X_1-2E[X_1]}) - T_{th}}{\sqrt{2N}}\right]$$

and

$$f_{\vec{X}}(\vec{X}) = \frac{1}{(2\pi)^{n/2} |C_X^{1/2}|} \cdot \exp\left(-\frac{1}{2} [(X_1 - E[X_1]) \dots (X_n - E[X_n])] \cdot C_X^{-1} \begin{bmatrix} (X_1 - E[X_1]) \\ \dots \\ (X_n - E[X_n]) \end{bmatrix}\right) \quad (4.11)$$

## 4.4 Free Space Optical Communications Systems Employing Subcarrier PSK

### 4.4.1 Free Space Optical Communications Systems Employing Subcarrier PSK Through Turbulent Atmospheric Channel for Log-normal PDF Channel

This section analyzes the performance of optical communication systems employing subcarrier PSK intensity modulation through the turbulent atmosphere. Consider the optical communication system employing subcarrier PSK intensity modulation in Fig. 1. In the electrical modulator, the data sequence is modulated using PSK, which can be implemented with existing microchips at very low cost. The PSK signal is unconverted to an intermediate frequency (IF)  $f_c$ . Because the bandwidth of the scintillation process  $A(u, t)$  is only a few kilohertz [25]. With the current RF technology,  $f_c$  can be large enough to support several gigabits per second. Unless required by a very high data rate,  $f_c$  should not be too large so that the terminal cost can be low. The upconverted PSK signal modulates the intensity of the laser in the transmitter. The transmitted optical intensity can be written as

$$s(t) = 1 + \alpha[s_i(t) \cos w_c t - s_q(t) \sin w_c t] \quad (4.12)$$

where  $s_i(t) = \sum_j g(t - jT_s) \cos \phi_j$  in the in-phase signal and  $s_q(t) = \sum_j g(t - jT_s) \sin \phi_j$  is the quadrature signal,  $0 < \alpha \leq 1$ ,  $w_c = 2\pi f_c$ ,  $\phi_j$  is the  $j$ th phase symbol,  $g(t)$  is the shaping pulse, and  $T_s$  is the symbol time. The amplitude satisfies  $\sqrt{s_i^2(t) + s_q^2(t)} \leq 1$  to avoid nonlinearity. Directly modulated laser diodes such as the JDS Uniphase CTR915 Series can be employed for high efficiency  $\alpha = 1$  and low cost. The dc component in the transmitted signal (22) is greater than zero, which is always true when intensity modulation is employed.

The received optical intensity can be written as

$$P(t) = I_o A(u, t) [1 + \alpha[s_i(t) \cos w_c t - s_q(t) \sin w_c t]] \quad (4.13)$$

Where  $I_o$  is constant. The electrical signal at the photodetector output can be written as

$$I(t) = A(u, t) + \alpha A[s_i(t) \cos w_c t - s_q(t) \sin w_c t] + n_i(t) \cos w_c t - n_q(t) \sin w_c t \quad (4.14)$$

where  $n_i(t)$  and  $n_q(t)$  are AWGN processes. The power spectral density of the received signal is

$$I(f) = A(f) + \frac{B(f - f_c) + B(f + f_c)}{2} + \frac{N(f - f_c) + N(f + f_c)}{2} \quad (4.15)$$

where  $B(f) = A(f) * Z(f)$ . Assume that  $f_c > B_A + B_B$  where  $f_c$  is the IP,  $B_A$  is the single-sided bandwidth of  $A_f$  and  $B_B$  is the single-sided bandwidth of  $B_f$ . The first term of in Eq. 4.14 can be filtered out by a bandpass filter, which gives the output

$$I_1(t) = \alpha A[s_i(t) \cos w_c t - s_q(t) \sin w_c t] + n_i(t) \cos w_c t - n_q(t) \sin w_c t \quad (4.16)$$

Downconverting this signal to the baseband gives the in-phase signal at the demodulator input as

$$r_i(t) = \alpha A(u, t)s_i(t) + n_i(t) \quad (4.17)$$

and the quadrature signal

$$r_q(t) = \alpha A(u, t)s_q(t) + n_q(t) \quad (4.18)$$

Taking  $\alpha = 1$  for optical communication systems employing BPSK through the log-normal atmospheric turbulence channel, the BER is

$$P_b = \int_0^\infty \frac{1}{\sqrt{\pi N}} \frac{1}{(2\pi\sigma_X^2)^{1/2}} \exp\left\{-\frac{\ln^2 x}{2\sigma_X^2}\right\} Q\left(\frac{\sqrt{2x}}{\sqrt{N}}\right) dx \quad (4.19)$$

where  $x = e^X$ . For optical communication systems employing QPSK through the log-normal atmospheric turbulence channel, the BER can be written as

$$P_b = \int_0^\infty \frac{1}{\sqrt{\pi N}} \frac{1}{(2\pi\sigma_X^2)^{1/2}} \exp\left\{-\frac{\ln^2 x}{2\sigma_X^2}\right\} Q\left(\frac{x}{\sqrt{N}}\right) dx \quad (4.20)$$

#### 4.4.2 Free Space Optical Communications Systems Employing Subcarrier PSK Through Turbulent Atmospheric Channel for Gamma-Gamma PDF Channel

For optical communication systems employing BPSK through the gamma-gamma atmospheric turbulence channel, the BER is

$$P_b = \int_0^\infty \frac{2(\alpha\beta)^{(\alpha+\beta)/2}}{\Gamma(\alpha)\Gamma(\beta)} I^{\frac{\alpha+\beta}{2}-1} K_{\alpha-\beta}(2\sqrt{\alpha\beta I}) Q\left(\frac{\sqrt{2}I}{\sqrt{N}}\right) dI \quad (4.21)$$

For optical communication systems employing QPSK through the gamma-gamma atmospheric turbulence channel, the BER can be written as

$$P_b = \int_0^\infty \frac{2(\alpha\beta)^{(\alpha+\beta)/2}}{\Gamma(\alpha)\Gamma(\beta)} I^{\frac{\alpha+\beta}{2}-1} K_{\alpha-\beta}(2\sqrt{\alpha\beta I}) Q\left(\frac{I}{\sqrt{N}}\right) dI \quad (4.22)$$

### 4.5 ML Detection of Q-Ary PPM in Turbulence Channels

#### 4.5.1 QPPM Modulation

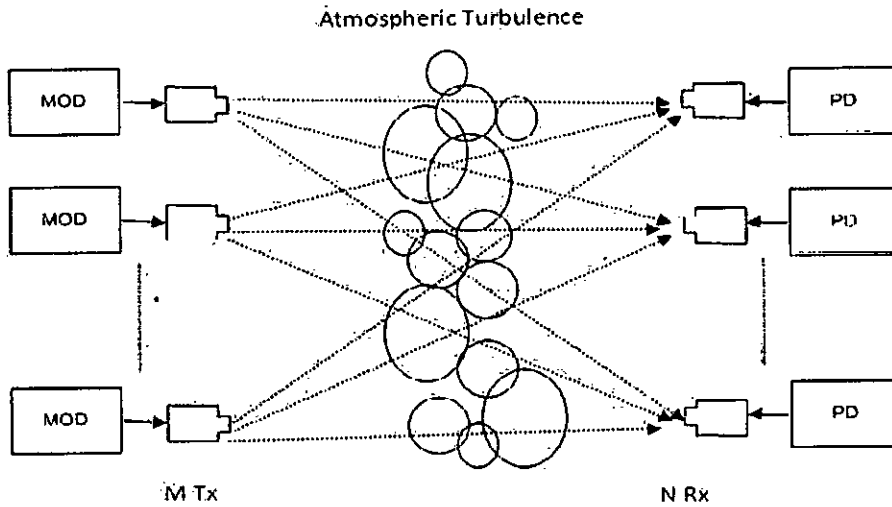


Fig. 4.3: Block diagram Q-ary PPM MIMO system

Earlier studies for optical space communication have shown that QPPM is an energy-efficient and readily implemented modulation choice for optical communication [34, 35]. In this method, a signaling interval of length is  $T_s$ , subdivided

into  $Q$  slots, each of length  $T = T_s/Q$  and a digital message comprised of  $\log_2 Q$  bits is sent by pulsing the laser in one of these slots. We assume that during the designated slot, the laser power, measured at the receiver after all link losses, is a constant  $P_r$  watts. Thus,  $P_r$  represents the peak power, and the received optical energy per symbol is  $E_s = P_r T$  joules. This can be related to the energy per information bit by  $E_b = E_s / \log_2 Q$ . The average power, when of interest, is  $P_r / Q$  watts. QPPM is advocated here over a simpler binary onoff modulation for another reason; the receiver does not require careful threshold adjustment that tracks the received power level to make optimal decisions. Gagliardi and Karp [34] conclude that under a total energy constraint, the optimal intensity pattern over slots is, in fact, that of PPM, i.e., fully on or fully off. They have studied the detection efficiency of QPPM for a single source/single detector channel, with and without background radiation. They also conclude that for a fixed  $E_b$ , and for no background radiation,  $Q$  is optimal in minimizing SEP. On the other hand, for high background radiation, large  $Q$  is preferred, since increasing  $Q$  shortens  $T$ , thus reducing the mean number of background photons per slot. A different set of conclusions is reached, however, if the comparison is made in terms of energy per bit; then we find that larger  $Q$  is always superior, and in the case that background radiation vanishes, we find that by letting  $Q$  become arbitrarily large, the energy per bit can decrease to zero while achieving any fixed BEP. The efficiency comes at the expense of large peak power, however, as well as large spectrum occupancy and additional synchronization difficulty with PPM.

To exploit the possibility of combating fading in optical links by use of multiple transmitters and/or receivers, we propose the following transmission setup. A  $Q$ -ary message is sent by simultaneously pulsing the same slot on the lasers, called repetition QPPM. The symbol interval remains at  $T_s$ , and the system communicates  $\log_2 Q$  bits per  $T_s$  seconds, as it would for a single-laser system. For fairness of comparison, we assume that the power available to a single-laser system is shared among the  $M$  lasers, and so  $P_r$  as above is the power presented to one PD by all lasers together. (This is the standard means of comparison in radio frequency (RF) MIMO analysis as well.) Of course, using multiple lasers is one way to increase total radiated power with constrained laser power; however,

we fix the total power (and energy) irrespective of  $M$ .

### 4.5.2 Optical Detection in QPPM

Most laser systems detect radiation with photo-detectors that are based on the photoelectric effect. Semiclassical radiation theory predicts, and is indeed based on the assumption, that the average rate of emission of photoelectrons by a photo-emitting surface which is irradiated with a constant intensity source of optical radiation is given by

$$\langle r \rangle = \frac{\eta I A_d}{hf} \quad (4.23)$$

where  $A_d$  is the detector surface area.  $\eta$  is the quantum efficiency of the detector, is the semiclassical parameter of the classical-wave concept of the intensity to the quantum mechanical concept of particle emission. It is generally identify as the probability of photoelectron emission given incident energy  $hf$ .

The statistics associated with photoemissive processes were originally developed by Purcell and Mandel within a semiclassical framework. We attempt to provide a simplified derivation of the probability density function for photoemission based on the probability  $P_k$  of  $K$  photoemissive events occurring in a finite time interval  $d\tau$ . From Eq. 4.24, the probability of an event occurring in a small time interval  $d\tau$  is  $\langle r \rangle d\tau$ , provided that  $d\tau$  is small enough that the probability of two or more events occurring during  $d\tau$  is negligible. The probability  $P_k(\tau + d\tau)$  is then the sum of two mutually exclusive occurrences:

1.  $k$  emission events occur by time  $\tau$  with probability  $P_k(\tau)$  and no events occur during the interval  $d\tau$ , the latter probability being  $(1 - \langle r \rangle \tau)$ . Since these events are independent by assumption, their joint probability is  $(1 - \langle r \rangle \tau)P_k\tau$ .
2.  $k - 1$  emission events occur in time  $\tau$  with probability  $P_{k-1}(\tau)$  and one emission occurs during the interval  $d\tau$ , the latter probability being  $\langle r \rangle d\tau$ . Once again, independence leads to a joint probability of  $\langle r \rangle d\tau P_{k-1}(\tau)$ .



Thus,

$$P_k(\tau + d\tau) = (1 - \langle r \rangle d\tau)P_k(\tau) + \langle r \rangle d\tau P_{k-1}(d\tau) \quad (4.24)$$

$$\frac{P_k(\tau + d\tau) - P_k(\tau)}{d\tau} = \langle r \rangle [P_{k-1}(\tau) - P_k(\tau)] \quad (4.25)$$

Letting  $d\tau \rightarrow 0$  yields

$$\frac{dP_k}{d\tau} = \langle r \rangle [P_{k-1}(\tau) - P_k(\tau)] \quad (4.26)$$

Assuming that  $k = 0$  emissions occur in the interval  $d\tau$  and  $P_{-1}(\tau) = 0$ , we have

$$\frac{dP_0}{d\tau} = -\langle r \rangle P_0(\tau) \quad (4.27)$$

Integrating with the boundary condition  $P_0(\tau) = 1$  yields

$$P_0(\tau) = e^{-\langle r \rangle \tau} \quad (4.28)$$

Similarly, for  $k = 1$  emissions in  $d\tau$ ,

$$\begin{aligned} \frac{dP_1}{d\tau} &= \langle r \rangle [P_0(\tau) - P_1(\tau)] \\ &= \langle r \rangle [e^{-\langle r \rangle \tau} - P_1(\tau)] \end{aligned} \quad (4.29)$$

With the boundary condition  $P_1(0) = 0$ , we obtain

$$P_1(\tau) = \langle r \rangle \tau e^{-\langle r \rangle \tau} \quad (4.30)$$

Continuing in this manner, it can be concluded by induction that

$$P_k(\tau) = \frac{(\langle r \rangle \tau)^k}{k!} e^{-\langle r \rangle \tau} \quad (4.31)$$

We therefore have for the average number of photoelectrons emitted in time  $\tau$

$$\bar{N} = \bar{r}\tau \quad (4.32)$$

where, for simplicity of notation, the averaging notation has been changed from brackets to overbars. Thus, using Eq. 4.31 in Eq. 4.32, while designating the function  $q()$  as a discrete probability density function, we obtain for the distribution of  $k$  photoelectrons,

$$q(k) = \frac{(\bar{N})^k e^{-\bar{N}}}{k!} \quad (4.33)$$

The Poisson density function of Eq. 4.33 represents the distribution of emitted photoelectrons during the counting interval  $\tau$ , where  $\bar{N}$  is the mean number of photoelectrons during  $\tau$ . In practice,  $\tau$  is identified with the measurement interval of the detection process, which for an optimally matched receiver, is the signal pulse width.

In addition to the signal there are several noise contributions to the photodetection statistics. Consider first those noise sources that are Poisson distributed. These can include background radiation due to solar scatter off clouds, terrain, or targets and detector dark currents. The latter arise when photoelectrons are thermally or quantum mechanically generated within the detector material.

Let  $n_s$  and  $n_b$  be the count variables representing the mean signal and noise photoelectrons, respectively. So probability mass function for the number of counts in an on interval is related to the optical intensity by the Poisson distribution

$$P(Z_{nq} = k) = \frac{(n_s + n_b)^k e^{-(n_s + n_b)}}{k!} \quad (4.34)$$

For detail analysis interested reader is referred to an the book by Osche G.R. [36].

If we designate the total incident power (spatial integral of the field intensity) at one PD as  $P_r$  watts, the effective count parameter of the Poisson count variable  $K$  is

$$n_s = \frac{\eta P_r T \sum_{m=1}^M x_{nm}^2}{hfM} \quad (4.35)$$

In addition to the desired signal, we presume the presence of a background optical field, again one whose bandwidth is wide and the effective count parameter

due to the background field is denoted as  $n_b$ . This is related to the total incident background power on one PD,  $P_b$ , by

$$n_b = \frac{\eta P_b T}{hf} \text{ photoelectrons/slot} \quad (4.36)$$

The poisson variants are independent, conditioned on the pulse pattern and channel gains, from slot-to-slot and across detectors. We designate the collection of counts by matrix  $Z = \{Z_{nq} = n = 1, 2, \dots, N, q = 1, 2, \dots, Q\}$

## 4.6 Performance Analysis for Log-normal Turbulence Channel

### A. No fading, No Background Radiation

First, consider the case of negligible background radiation and equal-gain links, i.e.,  $x_{nm} = 1$  almost surely,  $n = 1, \dots, N, m = 1, \dots, M$ . With no loss of generality, assume that each laser sends energy in slot 1. The only possibility for decision error is that each detector registers zero counts in time slot 1, since the other slots register zero counts by assumption  $n_b = 0$ . By the Poisson property and independence, we have SEP

$$P_s = \frac{Q-1}{Q} \left[ \exp^{-\frac{M\eta(\frac{E_s}{M})r_s}{hfQ}} \right]^N \quad (4.37)$$

This says that for a fixed total symbol transmitter energy, the probability of bit error is independent of  $M$ , i.e., there is no phased-array gain attached to the multiple sources, since these are noncoherent sources. The effective received power does increase, however, with  $N$ , which can be interpreted as the effect of increasing receiving aperture size, or increasing the optical gain.

Moreover, the SEP is independent of  $Q$  for a fixed energy per symbol. However, as  $Q$  increases for a fixed bit rate, the peak power must increase as  $Q/\log_2 Q$  to maintain fixed energy per symbol.

On this same theme, we may wish to focus upon the required energy per bit needed to achieve a given  $P_b$ . Since  $E_s = (\log_2 Q)E_b$  we have that the

required  $E_b$  can decrease as  $\log_2 Q$ , and, in fact, an arbitrarily small  $E_b$  can achieve any small  $P_b$ , as  $Q \rightarrow \infty$ . This, of course, presumes no background interference, and supposes unlimited peak power, so that all the symbol energy can be collapsed into a vanishingly small time interval.

### B. Fading, No Background Radiation

The probability of zero count in slot 1 at detector  $n$  is

$$P[Z_{n1} = 0 | \text{slot1}, X] = e^{-\sum_{m=1}^M x_{nm}^2 \left(\frac{\eta p_r}{M h_f}\right) \left(\frac{T_s}{Q}\right)} \quad (4.38)$$

and probability that all slot-1 counts are zero becomes

$$P[Z_{n1} = 0 | \text{slot1}, X] = e^{-\sum_{m=1}^M \sum_{n=1}^N x_{nm}^2 \left(\frac{\eta p_r}{M h_f}\right) \left(\frac{T_s}{Q}\right)} \quad (4.39)$$

If the path gains are independently distributed and identical, the average symbol error becomes

$$P_s = \int P_{s|X} f_X(x) dx = \frac{Q-1}{Q} \left\{ \left[ \int e^{-\frac{\eta x^2 E_s}{h_f M}} f_X(x) dx \right]^N \right\}^M \quad (4.40)$$

$$P_s = \frac{Q-1}{Q} \left\{ \left[ \int e^{-\frac{x^2 \eta \left(\frac{E_s}{h_f}\right)}{h_f}} \frac{1}{(2\pi\sigma_X^2)^{1/2}} \exp\left(-\frac{(\ln x - E[X])^2}{2\sigma_X^2}\right) dx \right]^N \right\}^M \quad (4.41)$$

### C. No Fading, Background Radiation

The upper bound of error probability [38] for this case

$$P_s = 1 - \left[ \sum_{i=1}^{\infty} \sum_{j=0}^{i-1} \frac{(N(n_s + n_b))^i e^{-N(n_s + n_b)}}{i!} \times \frac{(N n_b) j e^{-N n_b}}{j!} \right]^{Q-1} \quad (4.42)$$

The expanding the equation in Taylor series for small  $n_s/n_b$  we can reduce the equation to [39]

$$P_s \simeq \frac{Q-1}{2} \exp\left(-\frac{n_s^2}{4n_b}\right) \quad (4.43)$$

#### D. Fading, Background Radiation

There is no simple expression for this case [38]. Here

$$\begin{aligned}
 P_s &= \int P_{s|X} f_X(x) dx \\
 P_{s|X} &= 1 - \left[ \sum_{i=1}^{\infty} \sum_{j=0}^{i-1} \frac{[(\frac{n_s}{M} \sum \sum x_{nm}^2) + Nn_b]^i}{i!} \right. \\
 &\quad \left. \times \frac{e^{-(\frac{n_s}{M} \sum \sum x_{nm}^2) + Nn_b} (Nn_b)^j e^{-Nn_b}}{j!} \right]^{Q-1}
 \end{aligned} \tag{4.44}$$

### 4.7 Performance Analysis and Numerical Results for Gamma-Gamma Turbulence Channel

Four cases will be considered with or without channel fading, and with and without background radiation.

#### A. No fading, No Background Radiation

In this case, symbol error probability (SEP) is

$$P_s = \frac{Q-1}{Q} \left[ \exp^{-\frac{M\eta(\frac{P_r}{M})T_s}{h_f Q}} \right]^N \tag{4.45}$$

#### B. Fading, No Background Radiation

The probability of zero count in slot 1 at detector  $n$  is  $P\{Z_{n1} = 0 | \text{slot1}, I\} = e^{-\sum_{m=1}^M I_{nm} (\frac{\eta P_r}{M h_f}) (\frac{T_s}{Q})}$  and probability that all slot-1 counts are zero becomes  $P\{Z_{n1} = 0 | \text{slot1}, I\} = e^{-\sum_{m=1}^M \sum_{n=1}^N I_{nm} (\frac{\eta P_r}{M h_f}) (\frac{T_s}{Q})}$ . If the path gains are independently distributed and identical,

$$\begin{aligned}
 P_s &= \int P_{s|I} f_I(I) dI \\
 &= \frac{Q-1}{Q} \left\{ \left[ \int e^{-\frac{\eta I \frac{E_s}{M}}{h_f}} f_I(\bar{I}) dI \right]^N \right\}^M
 \end{aligned} \tag{4.46}$$

$$P_s = \frac{Q-1}{Q} \left\{ \left[ \int e^{-\frac{\eta I \frac{E_s}{M}}{h_f}} \frac{2(\alpha\beta)^{(\alpha+\beta)/2}}{\Gamma(\alpha)\Gamma(\beta)} I^{(\alpha+\beta)/2-1} K_{\alpha-\beta}(2\sqrt{\alpha\beta}I) dI \right]^N \right\}^M \tag{4.47}$$

### C. No Fading, Background Radiation

The upper bound of error probability [38] for this case

$$P_s = 1 - \left[ \sum_{i=1}^{\infty} \sum_{j=0}^{i-1} \frac{(N(n_s + n_b))^i e^{-N(n_s + n_b)}}{i!} \times \frac{(Nn_b)j e^{-Nn_b}}{j!} \right]^{Q-1} \quad (4.48)$$

The expanding the equation in Taylor series for small  $n_s/n_b$  we can reduce the equation to [39]

$$P_s \simeq \frac{Q-1}{2} \exp\left(-\frac{n_s^2}{4n_b}\right) \quad (4.49)$$

### D. Fading, Background Radiation

There is no simple expression for this case [38]. Here

$$P_s = \int P_{s|I} f_I(I) dI$$

$$P_{s|I} = 1 - \left[ \sum_{i=1}^{\infty} \sum_{j=0}^{i-1} \frac{[(\frac{n_s}{M} \sum \sum I_{nm}) + Nn_b]^i}{i!} \times \frac{e^{-(\frac{n_s}{M} \sum \sum I_{nm}) + Nn_b} (Nn_b)j e^{-Nn_b}}{j!} \right]^{Q-1} \quad (4.50)$$

# Chapter 5

## Result and Discussion

### 5.1 Introduction

The chapter is organized as follows. In Section 5.2 simulated performance results are illustrated and analyzed for OOK, taking the link as a log-normal channel. In this section, we also show that how diversity reception with two receivers can improve the performance as compared to a single receiver. In Section 5.3 simulated performance results are presented for both log-normal and gamma-gamma channel employing subcarrier BPSK and QPSK. It will be shown that BER performance of systems employing subcarrier BPSK is much better than that of compatible systems employing fixed-threshold OOK. In the last Section 5.4 the numerical results are presented and analyzed for both log-normal and gamma-gamma channel employing Q-ary PPM. It will be shown that if we increase the number of transmitters or receivers the performance of the system improves significantly.

For the convenience of the readers, the parameters used for computation in this chapter are shown in Table 5.1.

Table 5.1: System Parameters

Modulation	OOK, BPSK, QPSK, Q-PPM
Channel Type	Log-normal, Gamma-gamma
$\sigma_x$	0.1-0.8
$\eta$	.85 (OOK, Q-PPM) 1 (BPSK, QPSK)
R	100 Mbps

## 5.2 Performance analysis for OOK

### 5.2.1 Performance Analysis for OOK in Log-normal Turbulence Condition for Single Receiver

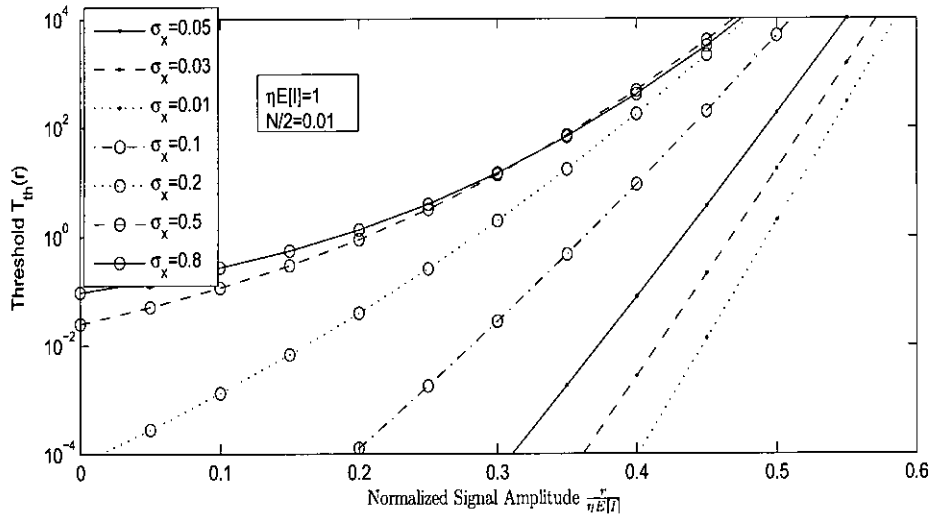


Fig. 5.1: Threshold versus normalized received signal amplitude for different values of the log-amplitude standard deviation for  $N/2=0.01$ .

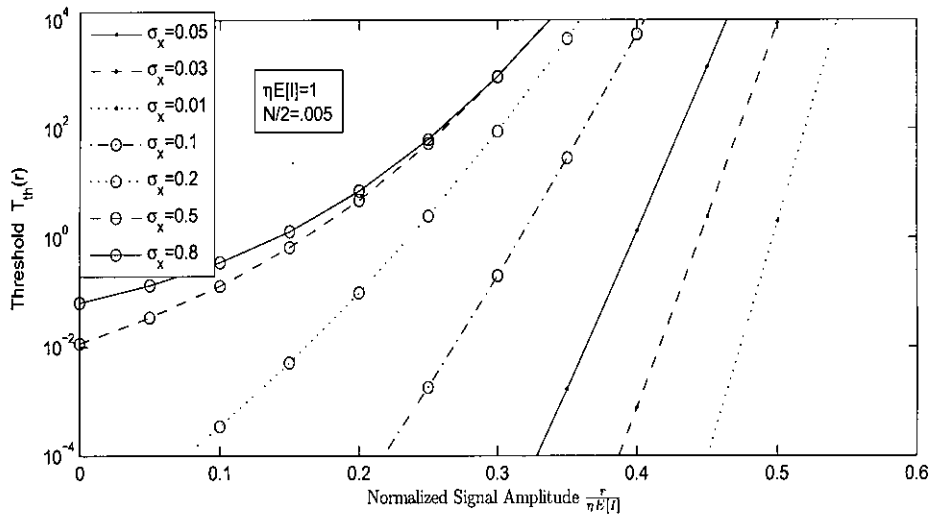


Fig. 5.2: Likelihood ratio versus normalized received signal amplitude for different values of the log-amplitude standard deviation for  $N/2=0.005$ .

In Fig. 5.1 and Fig. 5.2 we see that the likelihood ratio increases monotonically with for  $0 \leq r \leq 1$ . In Fig. 5.1 we plot threshold decision versus normalized



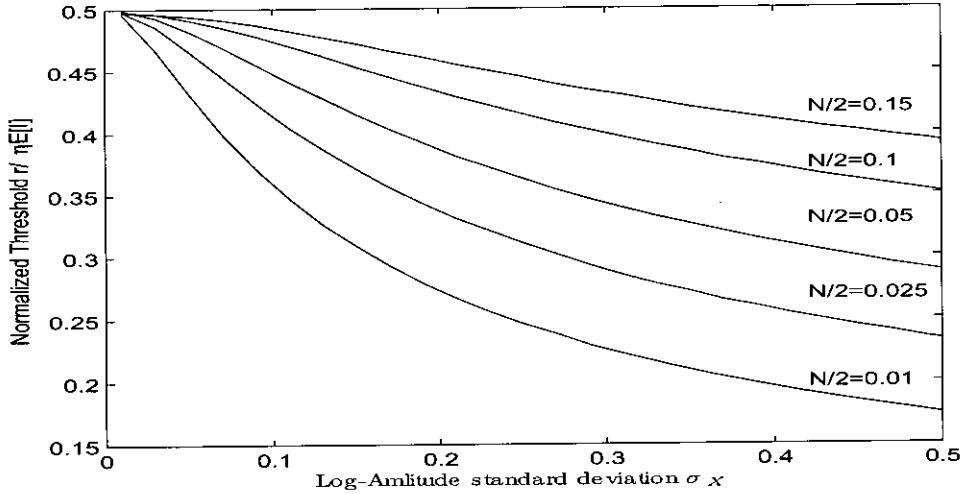


Fig. 5.3: Normalized threshold versus log-amplitude standard deviation for different values of the noise covariance.

signal amplitude for  $\sigma_X \in \{0.05, 0.03, 0.01, 0.1, 0.2, 0.5, 0.8\}$  considering additive Gaussian noise covariance  $N/2 = 0.01$ . In Fig. 5.2 we plot threshold decision versus normalized signal amplitude for  $\sigma_X \in \{0.05, 0.03, 0.01, 0.1, 0.2, 0.5, 0.8\}$  considering additive Gaussian noise covariance  $N/2 = 0.005$ .

In Fig. 5.3, we plot the optimal threshold for  $0 \leq r \leq 1$  versus the log-amplitude standard deviation  $\sigma_X$ . In this figure the additive Gaussian noise covariance is  $N/2 \in \{0.15, 0.1, 0.05, 0.025, 0.01\}$ . We see that as  $\sigma_X$  increases, the threshold decreases toward zero, because turbulence-induced fading increases the fluctuation of the On-state signal level, while leaving the fluctuation of the Off-state signal level unchanged.

In Fig. 5.3, we also see that as the additive Gaussian noise covariance  $N/2$  increases, the fluctuations of the Off and On states become more closely equal and the threshold increases toward  $1/2$ .

Fig. 5.4 shows the performance of single receiver for log-normal channel at different turbulence strength express in terms of  $\sigma_x$ . For this figure the log-amplitude variance  $\sigma_x \in \{0.1, 0.15, 0.2, 0.25\}$ .

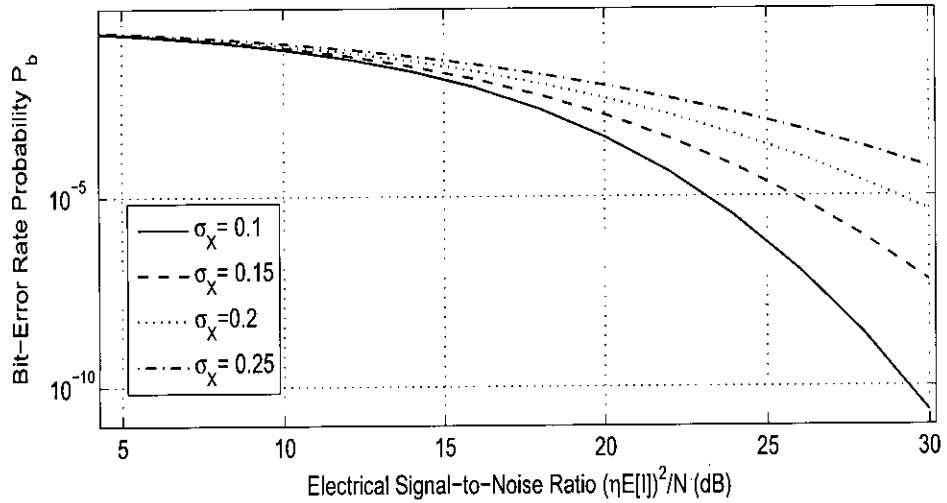


Fig. 5.4: BER vs average signal to noise ratio (SNR) for different  $\sigma_x$

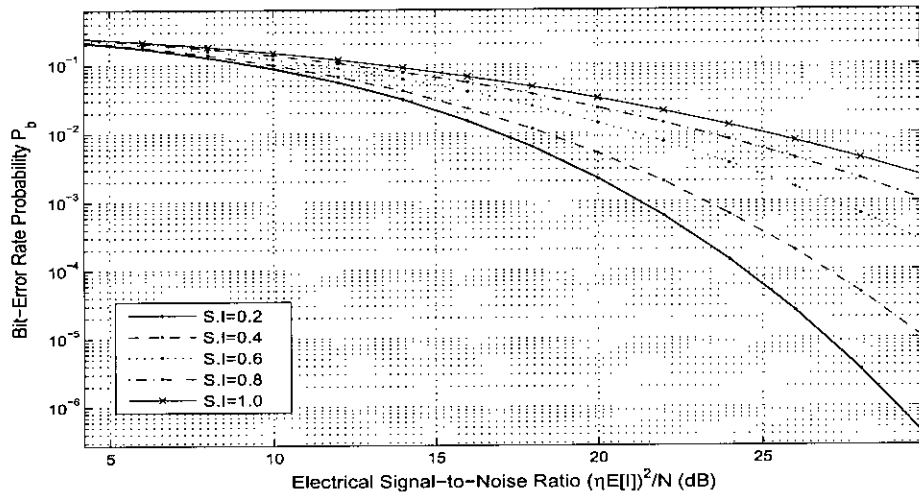


Fig. 5.5: BER vs average signal to noise ratio (SNR) for different S.I.

Fig. 5.5 show the performance of single receiver with the variation of  $S.I.$ . We see that turbulence-induced fading causes a greater degradation of the bit error probability when the standard deviation  $\sigma_x$  or scintillation  $S.I.$  is larger.

In the Fig. 5.6 we see to maintain a BER of  $10^{-6}$  we need higher SNR or higher signal power at higher scintillation index or higher  $\sigma_x$ .

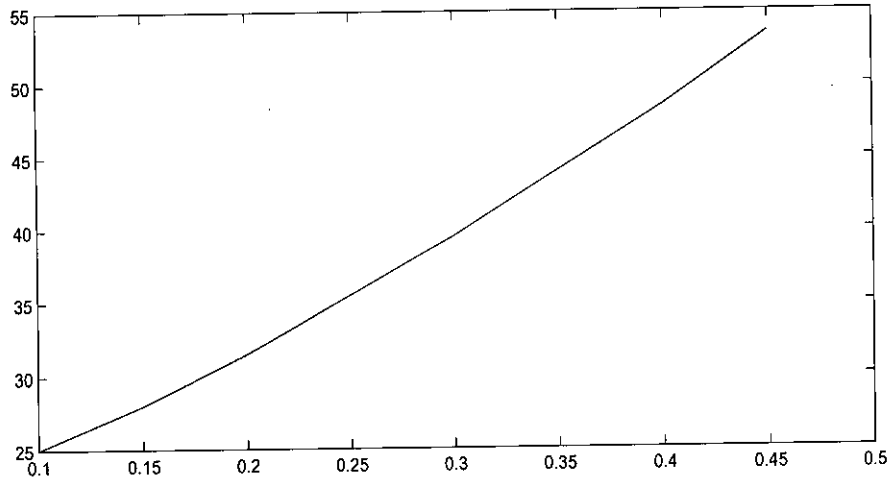


Fig. 5.6: Minimum SNR required for maintaining BER of  $10^{-6}$

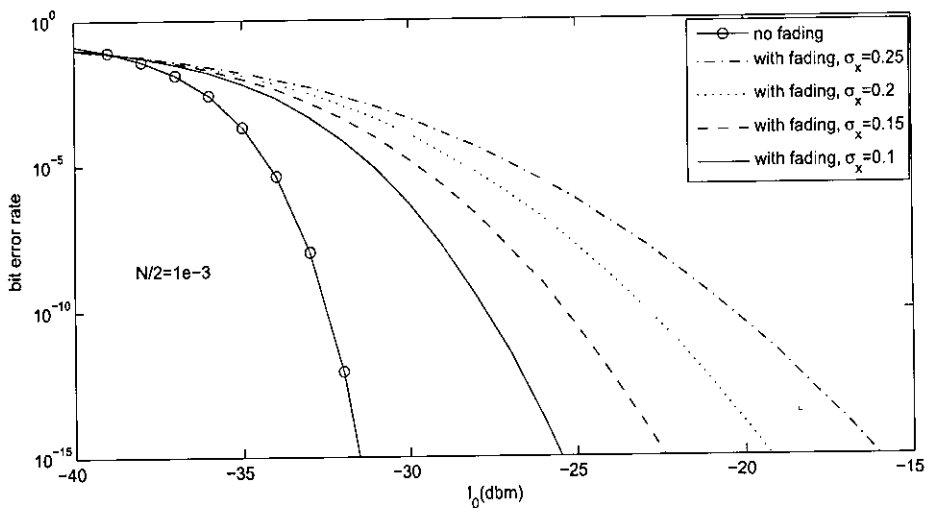


Fig. 5.7: BER vs  $I_0$  for different  $\sigma_x$  where  $N/2=0.001$

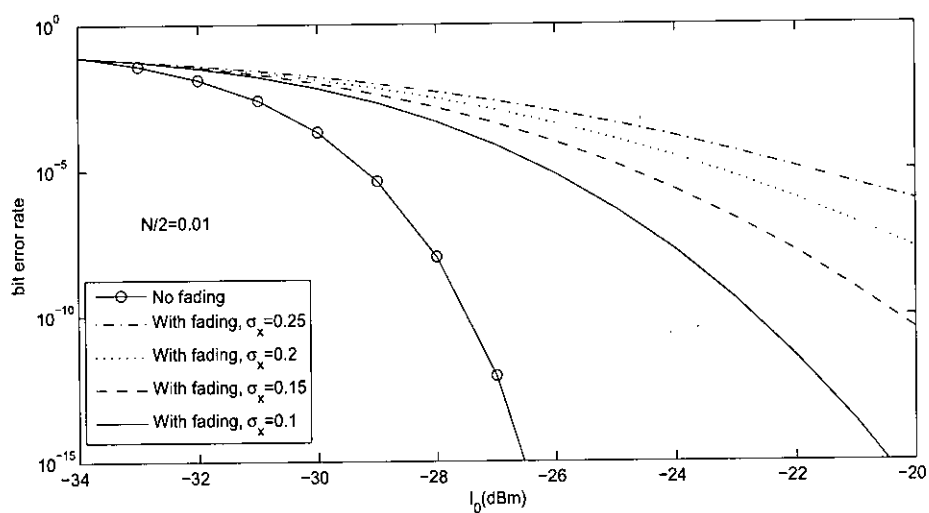


Fig. 5.8: BER vs  $I_0$  for different  $\sigma_x$  where  $N/2=0.01$

## 5.2.2 Performance Analysis for OOK in Log-normal Turbulence Condition for Dual Receiver

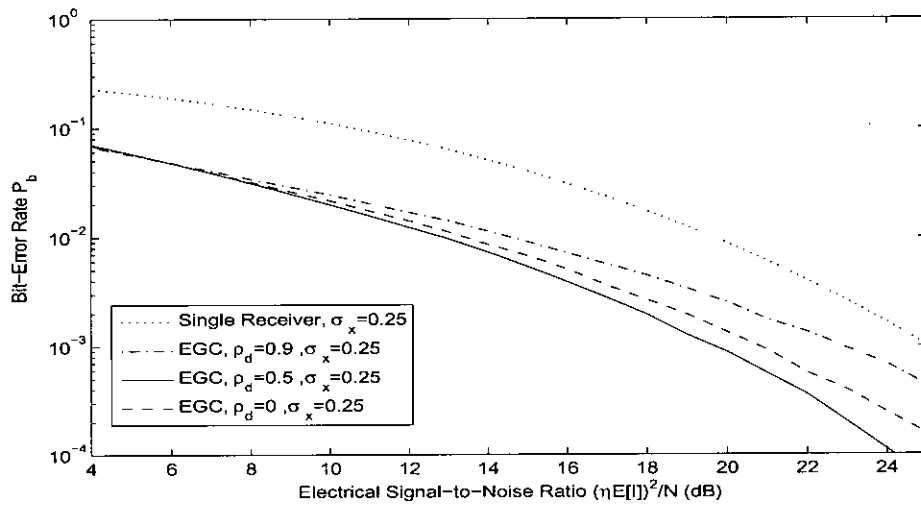


Fig. 5.9: Bit error rate of dual branch receiver versus signal-to-noise ratio using EGC receiver for different value of  $p_d$  for  $\sigma_x=0.25$

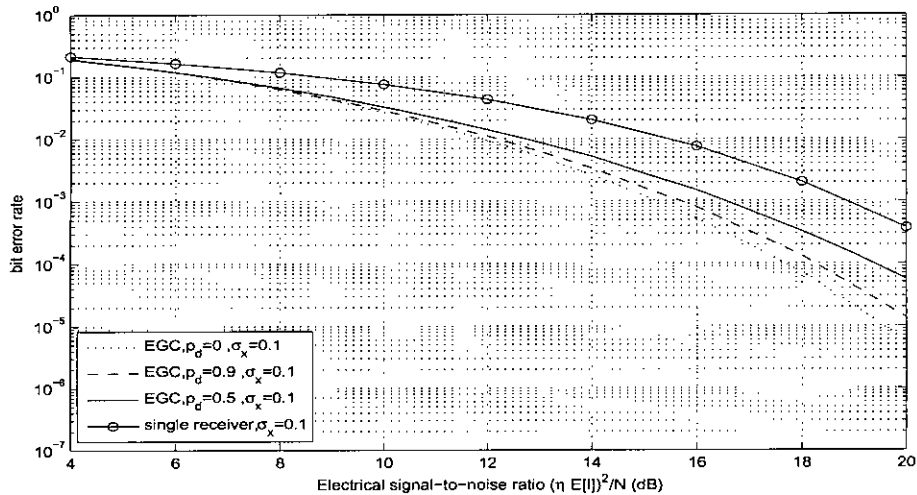


Fig. 5.10: Bit error rate of dual branch receiver versus signal-to-noise ratio using EGC receiver for different value of  $p_d$  for  $\sigma_x=0.1$

As described above, the EGC receiver [Fig. 4.2] has the knowledge of marginal distribution of fades at receivers. We assume that  $E[I_1] = E[I_2] = E[I]$  and  $N_1 = N_2 = N$ . In Fig.5.10 and Fig.5.9 we plot the simulation results, assuming

$E[X] = 0$  and  $\sigma_X$  is 0.25 and 0.1 correspondingly, varying the normalized correlation  $\rho_d = b_x(d_{12})$  from 0 to 0.9.

Diversity reception with two receiver can improve the performance as compared to the single receiver. Comparing Fig. 5.9 and Fig. 5.10 we see that the performance improvement in terms of BER is greater when the  $\sigma_x$  is larger.

## 5.3 Free Space Optical Communications Systems Employing Subcarrier PSK

### 5.3.1 Free Space Optical Communications Systems Employing Subcarrier PSK Through Turbulent Atmospheric Channel for Log-normal channel

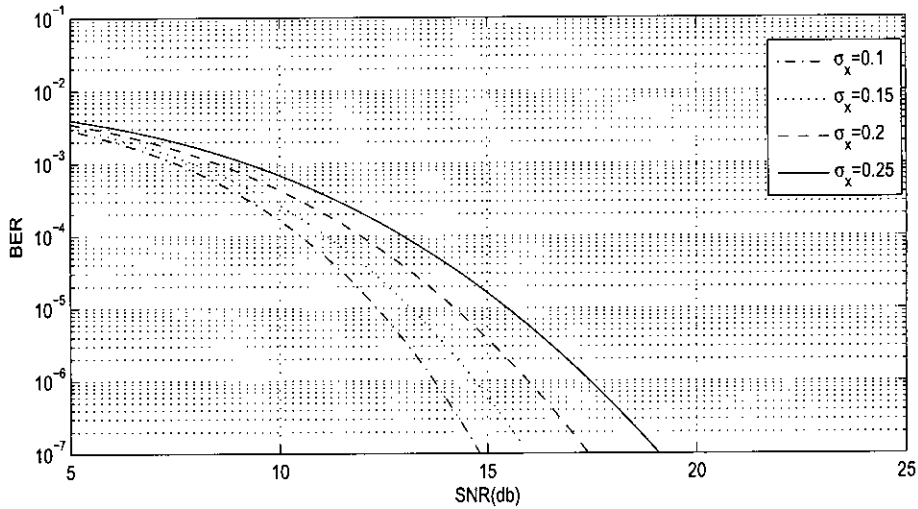


Fig. 5.11: BER performance of optical communication systems employing subcarrier BPSK for different  $\sigma_x$  for log-normal turbulence channel

Fig. 5.11 shows simulated BER for an optical communication system employing BPSK. The scintillation level is  $\sigma_x \in \{0.1, 0.15, 0.2, 0.25\}$ .

Fig. 5.12 shows simulated BER for an optical communication system employing BPSK. The scintillation index level is  $S.I \in \{0.1, 0.15, 0.2, 0.25\}$ .

Fig. 5.13 shows the minimum SNR required for maintaining BER of  $10^{-6}$  BPSK modulation scheme for log-normal turbulence channel. We see that if  $\sigma_x$  increases the required SNR is also increased almost linearly to maintain BER of  $10^{-6}$ .

In Fig. 5.14 and Fig. 5.15 we draw the BER curve for both BPSK and QPSK system for different strength of atmospheric turbulence.

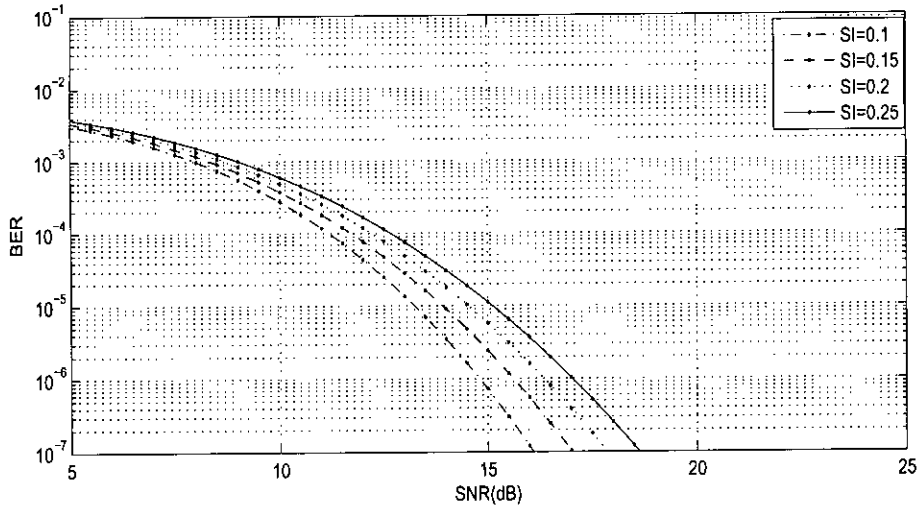


Fig. 5.12: BER performance of optical communication systems employing sub-carrier BPSK for different S.I. for log-normal turbulence channel

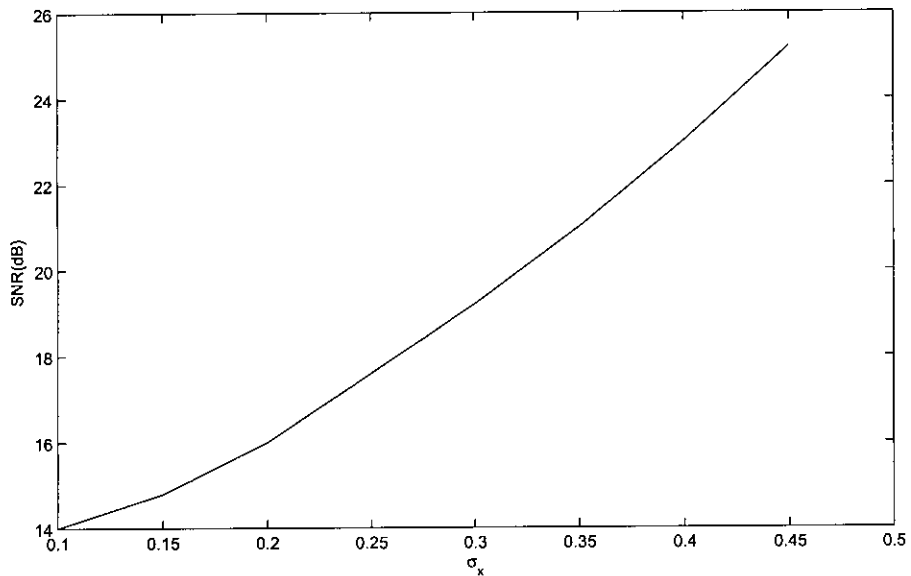


Fig. 5.13: Minimum SNR required for maintaining BER of  $10^{-6}$  BPSK modulation scheme for log-normal turbulence channel

In Fig. 5.17 minimum SNR required for maintaining BER of  $10^{-6}$  for different modulation scheme for OOK, BPSK, QPSK scheme. From the figure show that for BER of  $10^{-6}$  At the scintillation level  $\sigma_x = 0.1$ , subcarrier BPSK modulation scheme gives a gain of 11 dB over OOK and subcarrier QPSK modulation scheme



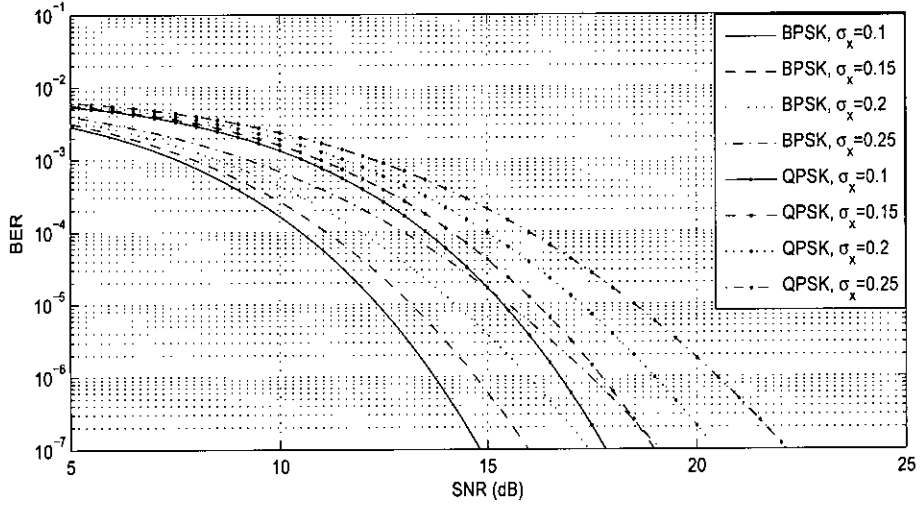


Fig. 5.14: Comparison of BER performance of subcarrier BPSK and subcarrier QPSK optical communication systems for different  $\sigma_x$  for log-normal turbulence channel

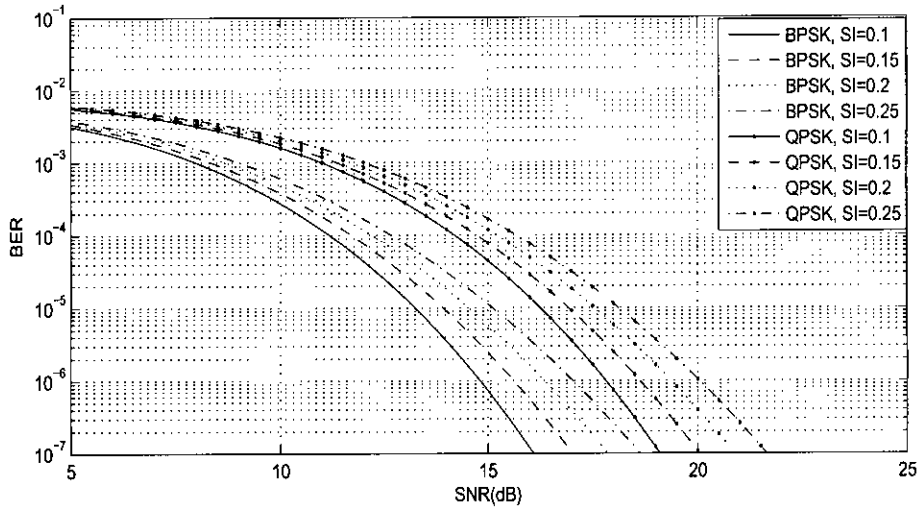


Fig. 5.15: Comparison of BER performance of subcarrier BPSK and subcarrier QPSK optical communication systems for different SI for log-normal turbulence channel

gives a gain of 8 dB over OOK. For higher level of  $\sigma_x$  the difference increases significantly but the difference between BPSK and QPSK modulation scheme is always 3 dB.

For subcarrier BPSK intensity modulation, the demodulator needs to estimate the received phase in  $\{0, \pi\}$ , and the equivalent demodulation threshold is zero.

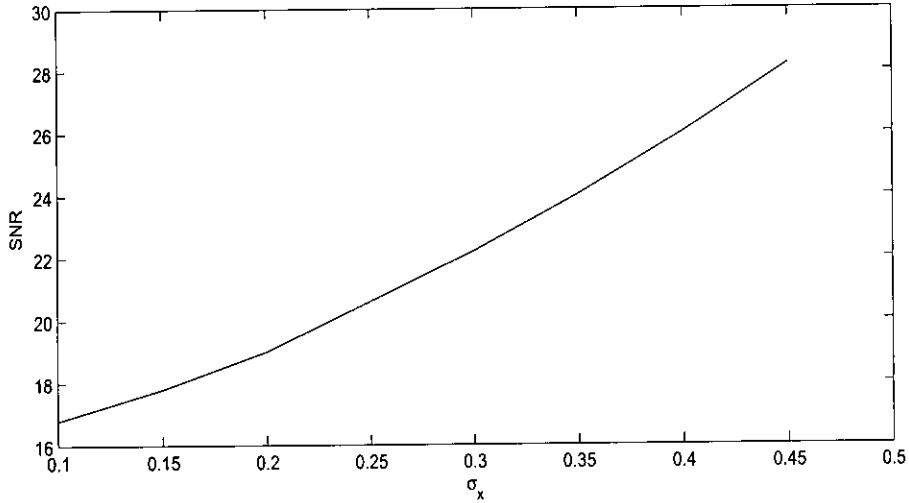


Fig. 5.16: Minimum SNR required for maintaining BER of  $10^{-6}$  for QPSK modulation scheme for log-normal turbulence channel

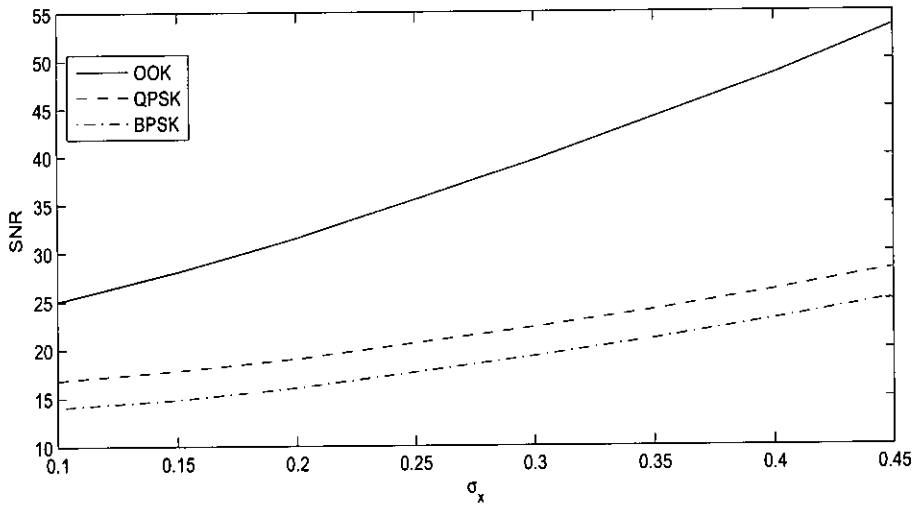


Fig. 5.17: Minimum SNR required for maintaining BER of  $10^{-6}$  for different modulation scheme for log-normal turbulence channel

When M-ary PSK with  $M \geq 4$  is employed, demodulation is in the phase domain, where the demodulator needs to estimate the phase among M possibilities. In the presence of scintillation, the subcarrier PSK modulation is more suitable than OOK because of the former's 0 threshold decision. For subcarrier M-ary PSK intensity modulation with  $M \geq 4$ , this claim is wrong. In general, it is the filtered-out dc response before demodulation that allows subcarrier PSK intensity

modulation to have superior demodulation performance. For M-ary PSK with  $M \geq 4$ , there does not exist any 0 threshold decision.

### 5.3.2 Free Space Optical Communications Systems Employing Subcarrier PSK Through Turbulent Atmospheric Channel for Gamma-Gamma Channel

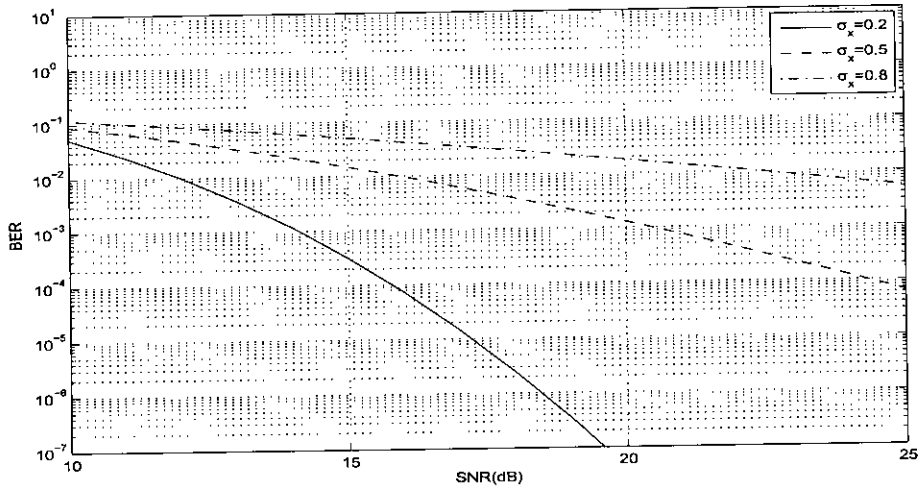


Fig. 5.18: BER performance of subcarrier BPSK optical communication systems for gamma-gamma turbulence channel

Fig. 5.18 shows simulated BER for an optical communication system employing BPSK. Here gamma-gamma channel is considered instead of log-normal channel. The scintillation level is  $\sigma_X \in \{0.2, 0.5, 0.8\}$ .

Fig. 5.19 shows simulated BER for an optical communication system employing QPSK for gamma-gamma atmospheric turbulence channel. The scintillation level is  $\sigma_X \in \{0.2, 0.5, 0.8\}$ .

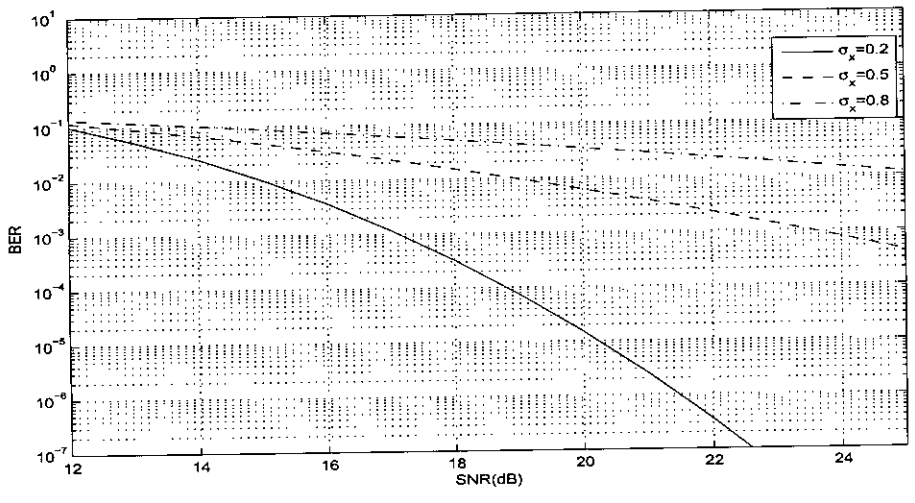


Fig. 5.19: BER performance of subcarrier QPSK optical communication systems for gamma-gamma turbulence channel

## 5.4 Performance Analysis for Q-ary PPM

### 5.4.1 Numerical Result and Discussion for Log-normal Channel

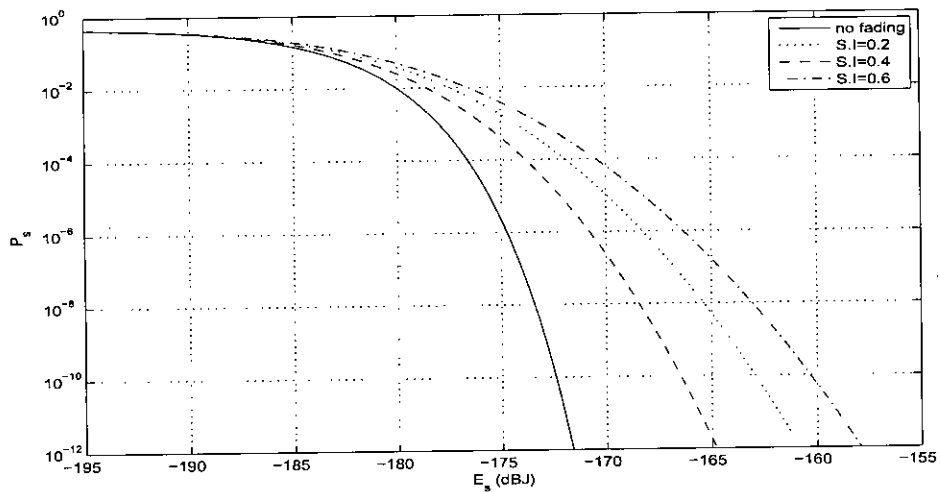


Fig. 5.20: Symbol-error probability, for  $Q=2, M=N=1$  and no background noise, for log-normal channel with different S.I

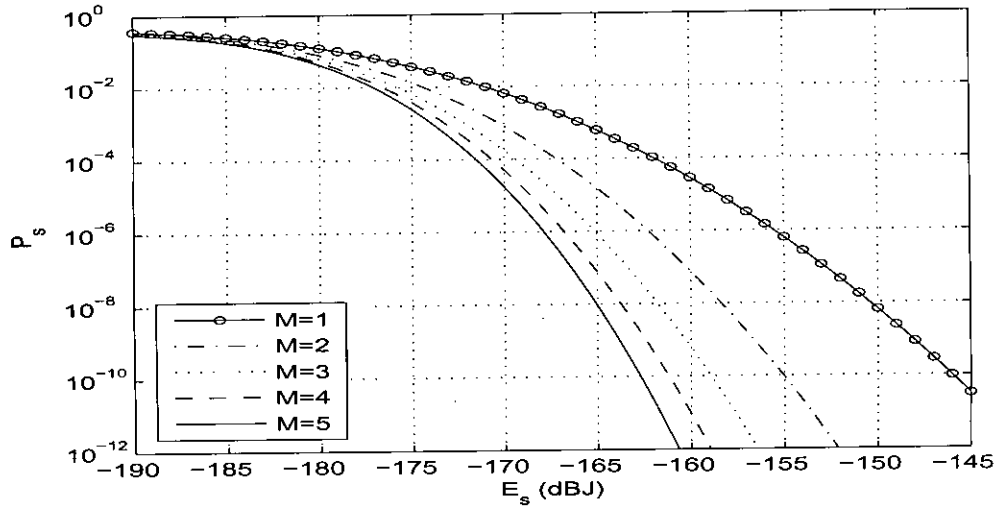


Fig. 5.21: Symbol-error probability with varying  $M$ , for  $Q=2, N=1$  and no background noise, for log-normal channel with  $\sigma_x = 0.6$

Fig. 5.21 shows the advantage of using multiple receive sensors in a log-normal faded channel.

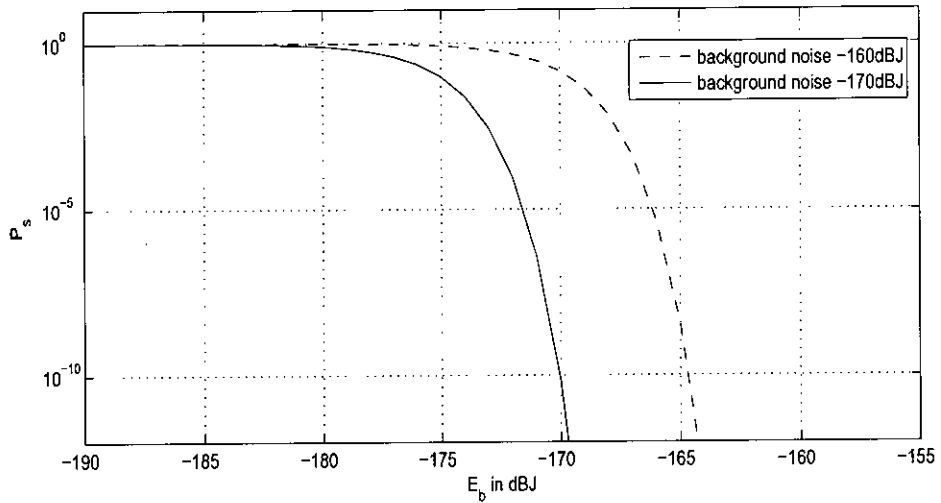


Fig. 5.22: Symbol-error probability for unfaded channel varying the bit rate, for a fixed background noise with  $M=1$  and  $N=1$ , for  $Q=2$

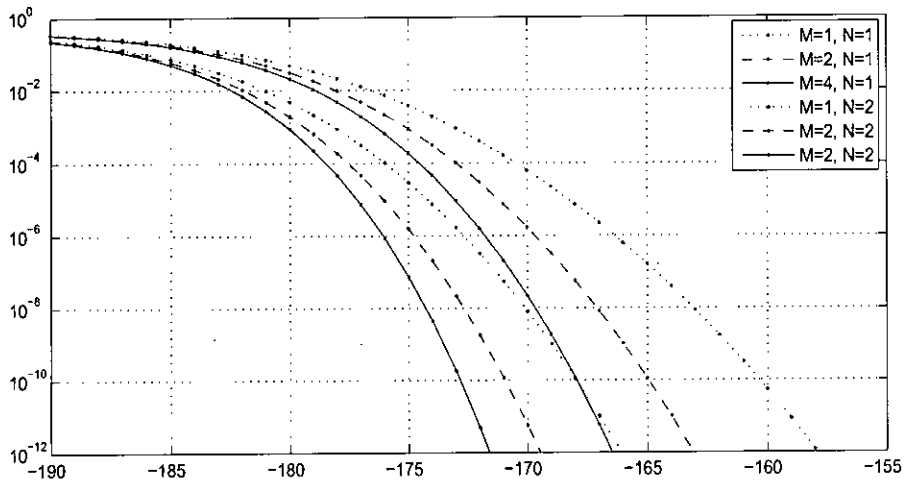


Fig. 5.23: Symbol-error probability for log-normal fading ( $\sigma_x = 0.6$ ), varying the number of Tx. and Rx., with background noise  $-170dBJ$ .

Fig. 5.23 presents performance for binary PPM with log-normal fading and fixed background radiation for an increasing number of transmitters and receivers. Comparing with the earlier performance plots, we clearly see the cumulative degradation imposed by fading and by background radiation. Adding elements to either the transmit or receive side does steepen the slope of the versus plot, and therefore, classical diversity is achieved.

## 5.4.2 Numerical Result and Discussion for Gamma-gamma Channel

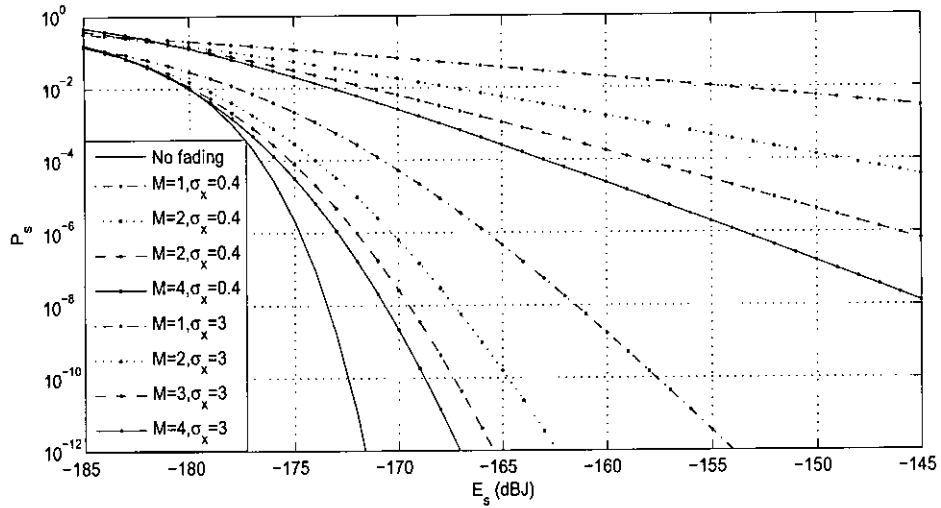


Fig. 5.24: Symbol-error probability with varying  $M$ , for  $Q=2, N=1$  and no background noise, for gamma-gamma channel with  $S.I = 0.4$  and  $S.I = 3.0$ .

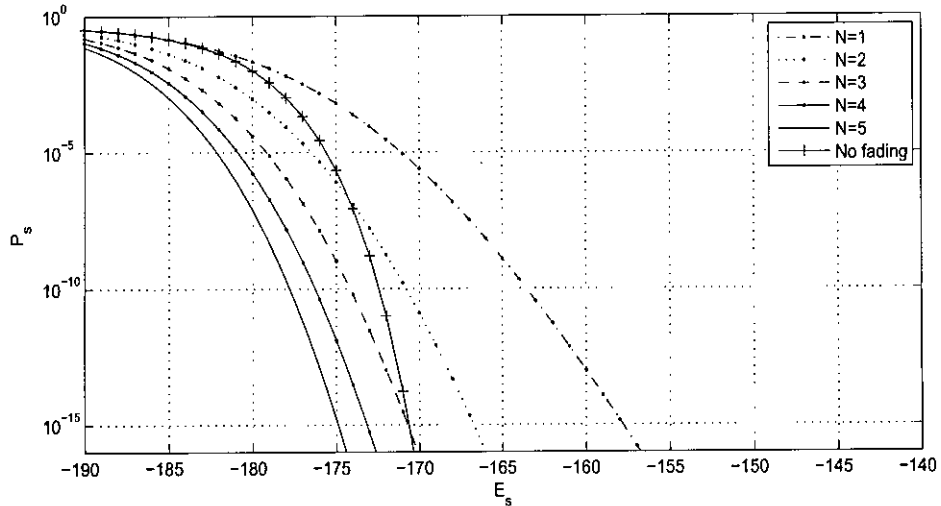


Fig. 5.25: Symbol-error probability with varying  $N$ , for  $Q=2, M=1$  and no background noise, for gamma-gamma channel with  $S.I = 0.4$ .

Fig. 5.24 shows the SEP  $P_s$  versus  $E_s$  where we have assumed quantum efficiency  $\eta = 0.5$ . Fig. 5.25 shows the advantage of using multiple receiver in gamma-gamma channel and Fig. 5.24 shows the advantage of using multi-



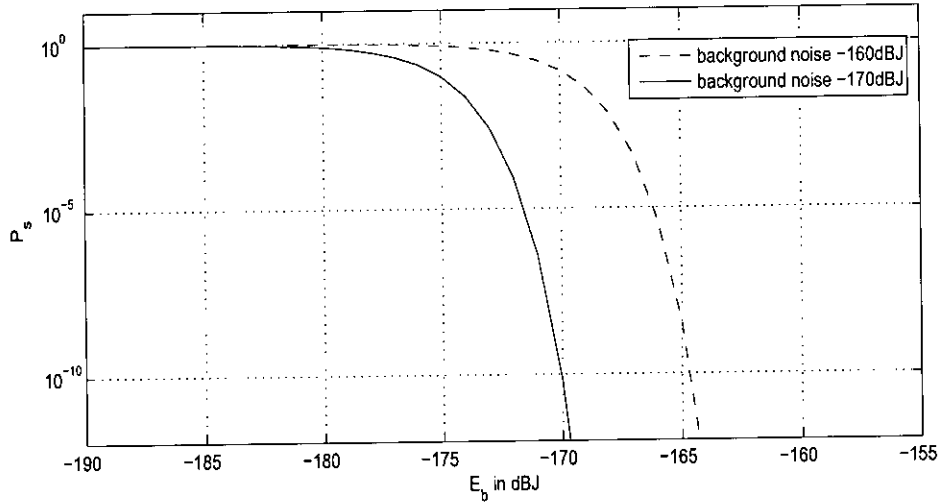


Fig. 5.26: Symbol-error probability for unfaded channel varying the bit rate, for a fixed background noise with  $M=1$  and  $N=1$ , for  $Q=2$

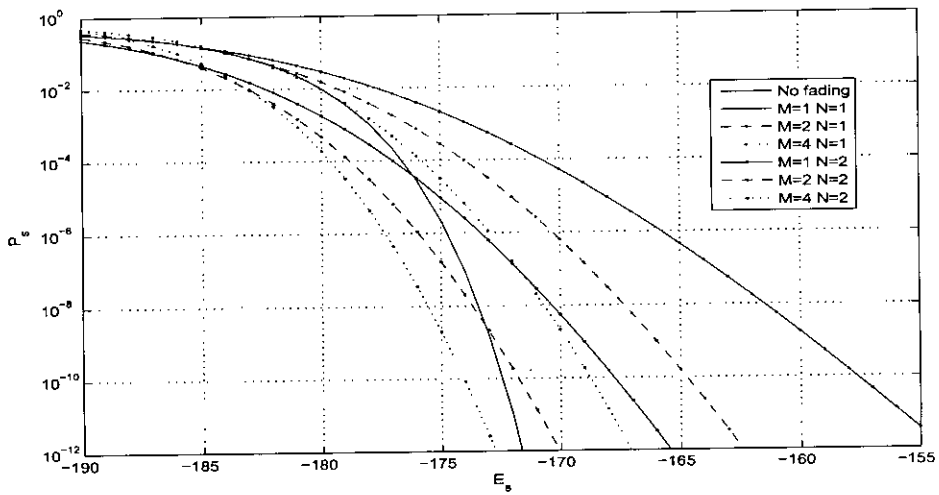


Fig. 5.27: Symbol-error probability for gamma-gamma fading ( $S.I = 0.4$ ), varying the number of Tx. and Rx., with background noise  $-170dB$ .

ple transmitter. Fig. 5.27 represents the SEP with gamma-gamma fading and fixed background radiation for different combination of multiple transmitter and receiver.

# Chapter 6

## Conclusion

### 6.1 Summary

A detailed analytical approach is presented to evaluate the bit error rate performance degradation of a wireless optical link in the presence of atmospheric scintillation with OOK, BPSK, QPSK and Q-ary PPM schemes. The analysis is extended for different turbulence channel like log-normal and gamma-gamma channel. The essential contributions and summary of the thesis are discussed below

- The gamma-gamma model approaches for heavy turbulence the exponential distribution, whereas in less turbulence it is suitable approximated by a log-normal distribution. To describe weak turbulence log-normal turbulence log-normal channel analysis is appropriate but moderate or heavy turbulence condition gamma-gamma channel is more appropriate to characterize the turbulence condition.
- It is found that the performance of FSO is very sensitive to atmospheric scintillation for all type of modulation schemes. There is a significant degradation in BER performance due to atmospheric scintillation and the penalty is higher for higher value of scintillation variation.
- Subcarrier M-ary PSK gives better performance than OOK. For subcarrier M-ary PSK intensity modulation with  $M \geq 4$ , this claim is wrong.
- Diversity reception with two receiver can improve the performance as compared to the single receiver. The performance improvement in terms of

BER is greater when the atmospheric turbulence is larger.

## 6.2 Scope of Future Research Work

- Different coding technique like convolution code, turbo code, LDPC, STBC can be applied to minimize the effect of atmospheric scintillation and scattering and to improve the performance of a free space optical communication system.
- Further research can be carried out on the effect of atmospheric scintillation for multi-hop FSO link.
- Research can be initiated to investigate the performance bounds of FSO link for different type of receiver in atmospheric turbulence.

# References

- 206005
- [1] V. W. S. Chan, "Free-space optical communications," *IEEE/OSA J. Light-wave Technol.*, vol. 124, no. 12, 1998.
  - [2] A. Acampora, "Last mile by laser," *Sci. Amer.*, vol. 287, pp. 48-53, Jul.2002.
  - [3] W. Goodman, *Statistical Optics*, New York: Wiley, 1985
  - [4] N. S. Kopeika, A. Zilberman, and Y. Sorani, , "Measured profiles of aerosols and turbulence for elevations of 2-20 km and consequences on widening of laser beams", *Proc. SPIE Optical Pulse and Beam Propagation III*, vol. 4271, 2001.
  - [5] X. Zhu, J. M. Kahn, "Free space optical communication through atmospheric turbulence channels," *IEEE Trans. on Communication*, vol. 50, no. 8, 2002.
  - [6] N. Cvijetic, S. G. Wilson, M. Brandt-Pearce, "Performance bounds for free-space optical MIMO systems with APD receivers in atmospheric turbulence," *IEEE J. Sel. Areas Commun.*, vol. 26, no. 3, 2008.
  - [7] I. B. Djordjevic, B. Vasic, M. A. Neifeld, "Multilevel coding in free-space optical MIMO transmission with Q-ary PPM over the atmospheric turbulence channel," *IEEE Photon. Technol. Lett.*, vol. 18, no. 14, 2006.
  - [8] S. Hranilovic, *Wireless Optical Communication System*, Springer, 2005.  
J. E. Padgett, C. G. Gunther and T. Hatori, "Overview of wireless personal communications," *IEEE Commun. Mag.*, vol. 33, no. 1, pp. 28-41, 1995.
  - [9] D. C. Cox, "Wireless personal communications: What is it?," *IEEE Personal Commun. Mag.*, vol. 2, no. 2, pp. 20-35, 1995.

- [10] R. Pandya, "Emerging mobile and personal communication systems," *IEEE Commun. Mag.*, vol. 33, no. 6, pp.44-52, 1995.
- [11] R. O. LaMaire, A. Krishna, P. Bhagwat and J. Panian, "Wireless LANs and mobile networking: Standards and future directions," *IEEE Commun. Mag.*, vol. 34, no. 8, pp. 86-94, 1996.
- [12] K. Pahlavan, A. Zahedi and P. Krishnamurthy, "Wideband local access: Wireless LAN and wireless atm," *IEEE Commun. Mag.*, vol. 35, no. 11, pp. 34-40, 1997.
- [13] J. M. Kahn and J. R. Barry. "Wireless infrared communications." *Proceedings of the IEEE*, 85(2):263-298, February 1997.
- [14] J. B. Carruthers and J. M. Kahn. "Modeling of nondirected wireless infrared channels". *IEEE Transactions on Communications*, vol. 45, no. 10, pp. 1260-1268, October 1997.
- [15] M. R. Pakravan, M. Kavehrad, and H. Hashemi. "Indoor wireless infrared channel characterization by measurements". *IEEE Transactions on Vehicular Technology*, vol. 50, no. 4, pp. 1053- 1073, July 2001.
- [16] S. Bloom, E. Korevaar, J. Schuster, and H. Willebrand. "Understanding the performance of free-space optics", *OSA Journal of Optical Networking*, vol. 2, no. 6, pp. 178-200, June 2003.
- [17] D. J. T. Heatley, D. R. Wisely, I. Neild, and P. Cochrane. "Optical wireless: The story so far", *IEEE Communications Magazine*, pages 72-82, December 1998.
- [18] G. Yun and M. Kavehrad, "Spot-diffusing and fly-eye receivers for indoor infrared wireless communications", *In Proceedings of the IEEE International Conference on Selected Topics in Wireless Communications*, pp. 262-265, 1992
- [19] J. B. Carruthers and J. M. Kahn, "Angle diversity for nondirected wireless infrared communication", *IEEE Transactions on Communications*, vol. 48, no. 6, pp. 960-969, June 2000.

- [20] V. Jungnickel, A. Forck, T. Haustein, U. Krger, V. Pohl, and C. von Helmolt, "Electronic tracking for wireless infrared communications." *IEEE Transactions on Wireless Communications*, vol. 2, no. 5, pp. 989-999, September 2003.
- [21] P. Beckmann, *Probability in Communication Engineering*, New York: Harcourt, Brace and World, 1967.
- [22] J. H. Churnside and S. F. Clifford, "Log-normal Rician probability density function of optical scintillations in the turbulent atmosphere", *J. Opt. Soc. Am. A*, vol. 4, no. 10, pp. 1923-1930, Oct. 1987.
- [23] T. Standage. *The Victorian Internet: the remarkable story of the telegraph and the nineteenth century's on-line pioneers* Walker and Co., New York, NY, 1998.
- [24] A. G. Bell. Selenium and the photophone. *Nature*, pages 500-503, Sept. 23, 1880.
- [25] F. R. Gfeler and U. Bapst, "Wireless in-house data communication via diffuse infrared radiation", *Proc. IEEE*, vol. 67, no. 11, pp. 1474-1486, 1979.
- [26] L. Andrews, R. L. Phillips and C. Y. Hopen, *Laser Beam Scintillation with Applications*, SPIE Press, 2001.
- [27] S. Karp, R. Gagliardi, S. E. Moran, and L. B. Stotts, *Optical Channels*, New York: Plenum, 1988.
- [28] A. Ishimaru, *Wave Propagation and Scattering in Random Media*, New York: Academic.
- [29] M. K. Simon and M.-S. Alouini, *Digital Communication Over Fading Channels: A Unified Approach to Performance Analysis*, New York: Wiley, 2000.
- [30] A. Consortini, R. Cochetti, J. H. Churnside, and R. J. Hill, "Innerscale effect on irradiance variance measured for weak-to-strong atmospheric scintillation," *J. Opt. Soc. Am. A* 10, pp. 2354-2362, 1993.

- [31] M. A. Al-Habash, L. C. Andrews and R. L. Phillips, "Mathematical model for the irradiance probability density function of a laser beam propagating through turbulent media", *Optical Engineering*, vol. 40, no. 8, pp. 1554-1562, August 2001.
- [32] G. L. Stuber, *Principles of Mobile Communication*, New York: Kluwer Academic, 1996.
- [33] J. G. Proakis, *Digital Communication*, 3rd ed. New York: McGraw- Hill, 1995.
- [34] R. Gagliardi and S. Karp, "M-ary Poisson detection and optical communications," *IEEE Trans. Commun. Technol.*, vol. 17, no. 4, pp. 208-216, Apr. 1969.
- [35] J. Lesh, "Capacity limit of the noiseless, energy-efficient optical PPM channel," *IEEE Trans. Commun.*, vol. 31, no. 4, pp. 546-548, Apr. 1982.
- [36] G. Ochse, *Optical Detection Theory for Laser Applications*, New York: Wiley-Interscience, 2002.
- [37] X. Zhu, J. M. Kahn, and J. Wang, "Mitigation of turbulence-induced scintillation noise in free-space optical links using temporal-domain detection techniques," *IEEE Photon. Technol. Lett.*, vol. 15, no. 4, pp. 623-625, Apr. 2003.
- [38] S. G. Wilson, M. Brandt-Pearce, Q. Cao, and J. J. H. Leveque III, "Free-space optical MIMO transmission with Q-ary PPM," *IEEE Trans. Commun.*, vol. 53, no. 8, pp. 1402-1412, Aug. 2005.
- [39] S. G. Wilson, M. Brandt-Pearce, Q. Cao, and M. Baedke, "Optical repetition MIMO transmission with multipulse PPM," *IEEE Sel. Areas Commun.*, vol. 23, no. 9, pp. 1901-1910, Sep. 2005.
- [40] X. Zhu, J. M. Kahn, "Communication techniques and coding for atmospheric turbulence channels" ,*J. Opt. Fiber. Commun. Rep.* , vol.4, pp. 363-405, 2007.

- [41] X. Zhu and J. M. Kahn, "Maximum-likelihood spatial-diversity reception on correlated turbulent free-space optical channels," *IEEE Conf. on Global Commun.*, San Francisco, CA, 2000.

